Effects of Sediment-Induced Density Gradients on the Estuarine Turbidity Maximum in the Yangtze Estuary

Zhu, Chunyan; van Maren, Dirk Sebastiaan; Guo, Leicheng; Lin, Jianliang; He, Qing; Wang, Zheng Bing

Important note
To cite this publication, please use the final published version (if applicable).
Please check the document version above.

Effects of Sediment-Induced Density Gradients on the Estuarine Turbidity Maximum in the Yangtze Estuary

Chunyan Zhu[1,2] , **Dirk Sebastiaan van Maren[1,2,3]**, **Leicheng Guo[1]** , **Jianliang Lin[1,2]**, **Qing He[1]** , and **Zheng Bing Wang[1,2,3]**

[1]State Key Lab of Estuarine and Coastal Research, East China Normal University, Shanghai, China, [2]Faculty of Civil Engineering and Geosciences, Delft University of Technology, Delft, the Netherlands, [3]Deltares, Delft, the Netherlands

Abstract An estuarine turbidity maximum (ETM) is a region of elevated suspended sediment concentration (SSC) resulting from residual transport mechanisms driven by river flow, tides, and salinity-induced density gradients (SalDG). However, in energetic and highly turbid environments such as the Yangtze Estuary, SedDG may also substantially contribute to the formation and maintenance of the ETM. Since this mechanism is relatively poorly understood, we develop a three-dimensional model to explore the effect of SedDG on tidal dynamics and sediment transport. By running sensitivity simulations considering SalDG and/or SedDG, we conclude that the longitudinal SedDG leads to degeneration and landward movement of the ETM. Moreover, two effects of the vertical SedDG are identified to be responsible for sediment trapping: One by enhancing the vertical sediment concentration gradients, and another by additionally affecting hydrodynamics including the water levels, velocities and salinities. The longitudinal and vertical SedDG leads to seasonal and spring-neap variations of upstream migration of the salt wedge: Vertical SedDG is more pronounced at neap tides in the wet season due to stronger stratification effects, whereas longitudinal SedDG is more pronounced at intermediate tides in the dry season due to weaker mixing and limited deposition. These findings imply that the SedDG contributes substantially to channel siltation and salt intrusion in highly turbid systems, and need to be accounted for when numerically modeling such phenomena.

Plain Language Summary In highly turbid estuaries, estuarine turbidity maximum (ETM) with high suspended sediment concentrations (SSC) influences the water quality and ecological system. These high SSCs interact with salinity, and the salinity and sediment transport influence siltation of navigation channels, freshwater resources and so on. In this study, we employ a three-dimensional numerical model to investigate the effect of sediment-induced density gradients (SedDG) on sediment transport and salt intrusion. The effects of the longitudinal and vertical SedDG weaken and promote the ETM (respectively), and influence salt intrusion. These findings are important for the management of sediment and freshwater resources in turbid estuaries.

1. Introduction

Many estuaries have regions with locally elevated suspended sediment concentration (SSC), which are referred to as an Estuarine Turbidity Maximum (ETM) (Dyer, 1986; Schubel, 1968). ETMs are areas with a convergence of sediment transport, often corresponding to the landward limit of salt intrusion. With high SSCs, the ETMs lead to dynamic bed behavior and may influence tidal propagation through damping of turbulence (Burchard & Baumert, 1998; Geyer, 1993; Talke & Jay, 2020). Understanding the dynamics of ETMs is important for the management of navigation channels, freshwater resources and ecosystem services.

ETMs reflect trapping of sediment in the longitudinal direction, often as a result of (at least one of) two main mechanisms: Tidal asymmetry and estuarine circulation. Tidal asymmetry is the distortion of the tidal wave resulting from non-linear interactions between the tide and channel morphology (Brenon & Le Hir, 1999; Dyer, 1988; Friedrichs & Aubrey, 1988; Uncles et al., 1985; Yu et al., 2014). Tidal wave distortion leads to stronger but shorter flood currents than ebb currents, resulting in a net transport of sediment in the landward direction. Estuarine circulation is characterized as a landward-directed bottom flow and a seaward directed surface flow, resulting from the baroclinic pressure gradient generated by longitudinal salinity differences (Burchard & Baumert, 1998; Dyer, 1988; Festa & Hansen, 1978; Geyer & MacCready, 2014).

Sediment is transported seaward in the surface layer, gradually settling from suspension toward the bottom layer, which transports sediment back in the landward direction. This two-layer flow exists seaward of the salt-fresh water interface, and therefore a resultant ETM will develop in the tip of the salt wedge. Moreover, internal tidal asymmetry due to the flood-ebb asymmetry in turbulent mixing is typically stronger during flood than ebb tides (Jay & Musiak, 1994, 1996). The reduction of tidal mixing during ebb tide results in internal tidal asymmetry that generates a two-layer tidally averaged residual circulation, which also contributes to estuarine circulation (Jay & Musiak, 1994, 1996). And finally, strain-induced tidal straining results from differential advection of a longitudinal density gradient (Simpson et al., 1990). During ebb tides, the water column is stratified via the straining of the density field which creates a vertically sheared velocity profile. During flood tides, this straining is reversed and the bottom water column becomes more mixed, intensifying the currents near the bottom. This asymmetric mixing leads to a residual flow strengthening the estuarine circulation (Jay & Musiak, 1994, 1996; MacCready & Geyer, 2010). Other than the above-mentioned mechanisms in inducing residual circulation in estuaries, in highly turbid estuaries, high SSC may result in extra density differences sufficiently large to dampen turbulent mixing, and therefore lead to rapid settling of suspended sediment, influencing the horizontal velocity structure (Winterwerp, 2001). Compared to the effect of salinity, the dynamics resulting from sediment-induced density differences have received much less scientific attention.

Sediment-induced density gradients (SedDG) may operate in both longitudinal and vertical directions and influence sediment trapping. Upstream of the location of the maximum SSC in the ETM, longitudinal salinity- and sediment-induced density gradients act together to enhance tidally averaged circulation (Talke et al., 2009). However, downstream of the maximum SSC in the ETM, the SedDG and salinity-induced density gradient (SalDG) may act in the opposite directions, leading to a three-layer circulation with near-bed seaward flow and therefore weakened residual currents (Talke et al., 2009). Additionally, SedDG promotes settling, resulting in larger gradients in the vertical SSC profile and more concentrated residual transport by depth-varying residual flows. And finally, vertical density gradients would suppress turbulence, reduce the apparent hydraulic roughness and lead to more amplified tides and enhanced tidal strength (Gabioux et al., 2005; Wang et al., 2014; Winterwerp et al., 2009), which in turn influence the ETM. Such a positive feedback may lead to an increase in SSC as a result of deepening and narrowing of navigation waterways in estuaries (de Jonge et al., 2014; van Maren, Winterwerp, & Vroom, 2015; Winterwerp, 2010; Winterwerp & Wang, 2013; Winterwerp et al., 2013). Moreover, the effect of sediment on the density causes variations in turbulence, and thereby mud-induced periodic stratification (Becker et al., 2018), leading to net upstream sediment transport, which is similar to the strain-induced periodic stratification (Simpson et al., 1990). But despite increasing phenomenological insight into the importance of sediment-induced effects, an integral study on the effects of the longitudinal and vertical SedDG on mixing, residual flows, and tidal propagation is still missing.

The Yangtze Estuary provides a case study in which all the above-mentioned dynamic processes play a role. It is an energetic and highly turbid estuary under strong fluvial and tidal forcing. An ETM stretching about 60 km in the mouth zone of the Yangtze Estuary occupies the region of the North and South Passages where bottom SSC can be >10 kg/m³ (Lin et al., 2019). The dynamics controlling the formation of ETM in the Yangtze have been extensively studied based on field observations (Li & Zhang, 1998; Song et al., 2013; Wu et al., 2012) and numerical models (Chu et al., 2010; Song & Wang, 2013; Wan & Wang, 2017). Figure 1 provides an example of high near-bottom SSC of ∼30 kg/m³ (∼1 m thick) lasting for 3–4 h in the middle of the North Passage (NP) (see Figure 2). The dynamics of these high concentration layers are regulated by the tidal variation in vertical mixing and horizontal advection, but their relative contribution remains poorly known. Even more, the impact of high near-bottom SSC on the hydrodynamics themselves (through its effect on the density, as elaborated above) remains poorly known. Earlier works suggest that the SedDG enhances stratification and strengthens the ETM (Li et al., 2018; Song & Wang, 2013; Wan & Wang, 2017) and leads to a lower apparent roughness (Winterwerp et al., 2009). However, these studies do not account for longitudinal SedDG which may behave differently than the vertical SedDG. The interactions between sediments, salinity, mixing and residual flows require further detailed analysis.

In this contribution, we aim at identifying the contribution of longitudinal and vertical SedDG and SalDG on ETM dynamics. A three-dimensional (3D) model is used to account for the effects of SalDG and SedDG
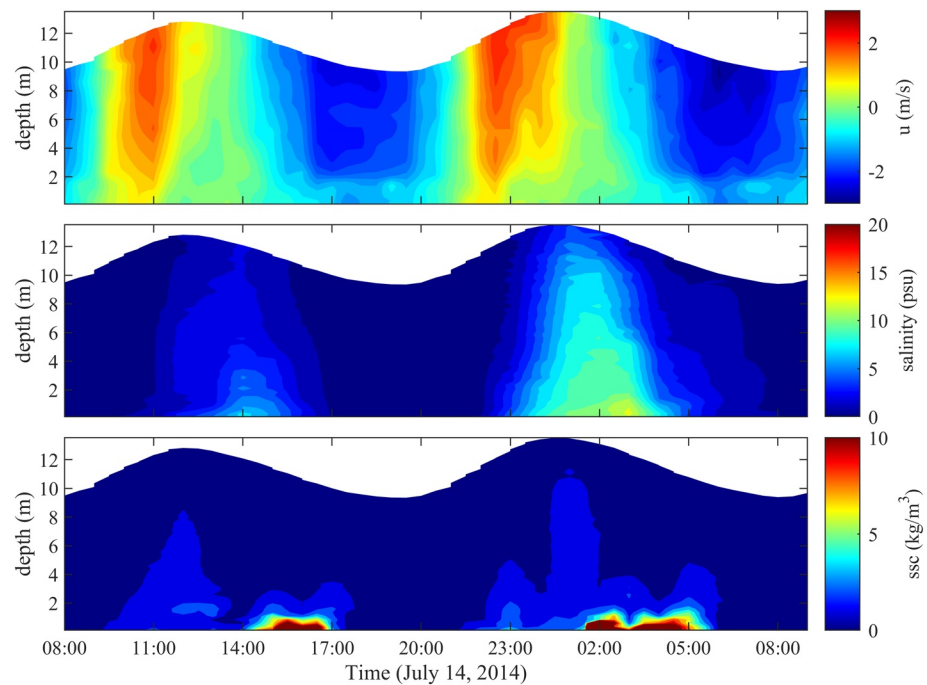
Figure 1. Observed variations of (a) Longitudinal velocity u; (b) Salinity and (c) Suspended sediment concentration (SSC) in the middle of the North Passage (see Figure 2) during July 14–15, 2014. Positive u indicates the flood direction. See Lin et al., (2019) for details.

individually as well as the interactions between the sediments and salinity. We systematically analyze the changes in the estuarine hydrodynamics, for example, the tidal propagation, residual flows, and stratification which contribute to the formation of the ETM. The setup of the model is described in Section 2, and model results are presented in Section 3. The model limitations, the effects of longitudinal and vertical Sed-DG, and the implications for other estuaries are discussed in Section 4. Conclusions are drawn in Section 5.

2. Methodology

2.1. Study Area

The Yangtze Estuary is a meso-tidal estuary (a mean tidal range of 2.6 m at the mouth but with spring tidal range up to 5.9 m) originating at Xuliujing (the estuary head, defined as 0-km) with four main outlets called the North Branch, the North Channel, the NP and the South Passage (Figure 2). It has a predominantly semi-diurnal tidal regime with M_2 as the most important component, followed by S_2, O_1, and K_1. The M_2 tidal amplitude increases in the first 50 km of the estuary due to the decreasing water depth and the convergent channel geometry. Further inside the estuary, the M_2 tidal amplitude decreases due to the damping effect of bottom friction and river discharge. The river discharge is high (monthly averaged value varying between 10,000–80,000 m^3/s at the tidal limit Datong station, 640 km upstream of the mouth). Wind and waves are of secondary importance compared to the river and tidal forcing. The river also supplies a huge amount of sediment (364 million tons per year during 1950–2016, Zhu et al., 2019) to the estuary. The river-borne sediment is fine, with a median grain size of 4–11 µm (Guo & He, 2011), whereas the bottom sediment in the estuary is relatively coarser, with a median grain size of 8–120 µm (Hu et al., 2009). The ETM in the Yangtze Estuary encompasses the region of the NP, South Passage and the seaward segment of the North Channel (C. Jiang et al., 2013; X. Jiang et al., 2013; Li & Zhang, 1998). Generally, the spatial extent of ETM varies with the river discharge (Doxaran et al., 2009) and sediment input (C. Jiang et al., 2013; X. Jiang et al., 2013).

The NP, where the ETM of the Yangtze Estuary is most pronounced, typically has a surface SSC of 0.1–0.3 kg/m^3 and a near-bottom SSC of 0.4–4 kg/m^3 varying with spring and neap tides as well as over wet
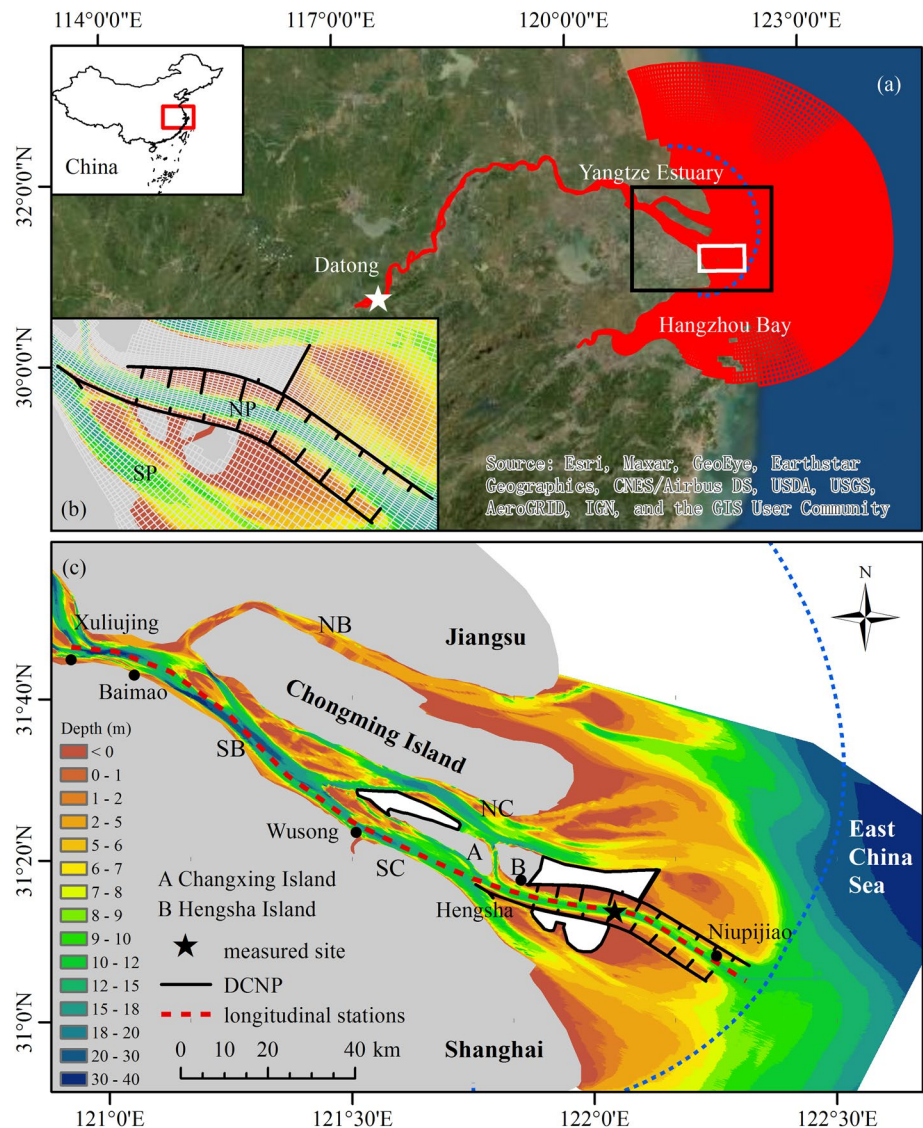
Figure 2. (a) Model domain; (b) Highest grid resolution in the mouth zone of the Yangtze Estuary; (c) Geometry and bathymetry of the Yangtze Estuary in 2010 and stations in the longitudinal direction (red dashed line). Seaward of the blue dashed line in (a) and (c) is prescribed as offshore settlings. The white areas are the reclaimed regions. DCNP, Deep Channel Navigation Project; NB, North Branch; SB, South Branch; NC, North Channel; SC, South Channel; NP, North Passage; SP, South Passage.

and dry seasons (Li et al., 2016; Liu et al., 2011; Shi, 2004). The near-bottom SSC, however, may exceed 10 kg/m^3 (see Figure 1, Lin et al., 2019) and even reach 100 kg/m^3 (Wan et al., 2014). Mixing and stratification periodically varies with the strength of river flow and tidal flow, leading to flood-ebb, spring-neap and seasonal variations (Li et al., 2016, 2018; Pu et al., 2015; Shi, 2004; Song et al., 2013; Wu et al., 2012). From 1998 to 2010, the NP was deepened and narrowed as part of the Deep Channel Navigation Project (DCNP) to accommodate larger ships. The DCNP was implemented with two long jetties and 19 groins to increase current velocity and mitigate sediment deposition in the main navigation channel. The main navigation channel was 350–400 m wide and 12.5 m, requiring an annual dredging volume of ∼50–60 million m^3 (Zhu et al., 2019). The high maintenance dredging costs fuels research on determining mechanisms controlling sediment trapping and siltation (C. Jiang et al., 2013; X. Jiang et al., 2013; Kuang et al., 2014; Liu et al., 2011; Wu et al., 2012). In this study, we focus on tidal propagation and sediment dynamics along the South Branch-South Channel-NP (see red dashed line in Figure 2).

Table 1
Parameter Settings in the Model (Details Refer to the Supporting Information)

Parameter	Description	Value
Δt (min)	Time step	0.5
n (s/m$^{-1/3}$)	Manning coefficient	0.01–0.025 with spatial variation
$\omega_{s,0}$ (mm/s)	Settling velocity	0.5
c_{soil} (kg/m^3)	Reference density for hindered settling	200
ρ_s (kg/m^3)	Specific density for cohesive sediment	2650
τ_{cr} (N/m^2)	Critical erosion stress	0.1
M (kg/m^2/s)	Erosion parameter	0.001

2.2. Model Setup

A 3D model was set up using the Delft3D model system (Lesser et al., 2004), which simulates flow, sediment transport and morphological changes. The model solves the three-dimensional shallow water equations under the hydrostatic pressure assumption—see Lesser et al. (2004) for details. Vertical mixing is computed with a k- ε turbulence model. The model application domain is about 700 km long and 400 km wide, covering the entire tidal region of the Yangtze River, the Hangzhou Bay and a part of the adjacent Yellow Sea and East China Sea (Figure 2). The model has 1,173 × 374 cells with a high resolution in the estuary (down to ∼300 m in the NP) and coarsening toward the river and the open sea (up to 10 km). Ten equidistant σ layers are prescribed over the vertical. The model is set up with a bathymetry measured in 2010 and calibrated with data collected in 2007, assuming that the bathymetry did not significantly change between 2007 and 2010. This assumption is reasonable as the impact of the DCNP construction (1997–2010) was most pronounced in the period 1997–2007 (see Zhu et al., 2019). Here we briefly describe the setup of the model: More details on the governing equations and the calibration are in the supporting information (SI).

2.2.1. Hydrodynamic Boundary Conditions

The upstream boundary is at Datong where a daily river discharge is prescribed with strong seasonal variations. A constant discharge of 1,000 m^3/s was defined at the head of Hangzhou Bay. At the seaward side, water levels are prescribed with 13 astronomic tidal constituents (M$_2$, S$_2$, N$_2$, K$_2$, K$_1$, O$_1$, P$_1$, Q$_1$, MF, M$_4$, MS$_4$, and MN$_4$) derived from the TPXO 7.2 Global Inverse Tide Model (Egbert & Erofeeva, 2002; Egbert et al., 1994) as a non-reflective open boundary. The tidal waves can across the open sea boundary unhampered and without reflections. The shallow water equations are solved by the steady-state solution which means the specified water level boundary acts as a nodal point. The salinity at the sea boundary is set constant and equal to 34 psu, whereas fresh water is prescribed at the upstream boundary. Although the Yangtze discharges a large amount of fresh water into the coastal seas, the model boundaries are sufficiently far away from the river mouth to allow a constant salinity value representing marine conditions. The model was first run for one year (2006) as a spin-up period, while the second year (2007) was used for calibration and detailed analysis. The 3D baroclinic model was calibrated with spatially varying Manning's n coefficient. The initial Manning's n (s/m$^{-1/3}$) was based on the roughness height in a calibrated hydrodynamic model (Zhu et al., 2016), which is subsequently optimized through calibration. In 2010, jetties and groins were constructed in the DCNP. These jetties and groins are numerically implemented as structures completely blocking through- or overflow. The calibrated parameters are summarized in Table 1.

2.2.2. Sediment Transport

The measured daily SSC, varying between 0.01 and 1 kg/m^3, was prescribed as a sediment transport boundary condition at Datong. The sediment concentration at the head of Hangzhou Bay is prescribed as zero. This is justified as the river sediment input here is negligible compared to the Yangtze River and seldom reaches the Yangtze Estuary (Hu et al., 2000). The sediment is represented by a single cohesive sediment fraction with a settling velocity of 0.5 mm/s (Yun, 2004). Sediment is modeled as supply limited: The model is not initialized with sediment on the bed, but sediment is transported into the model through the open
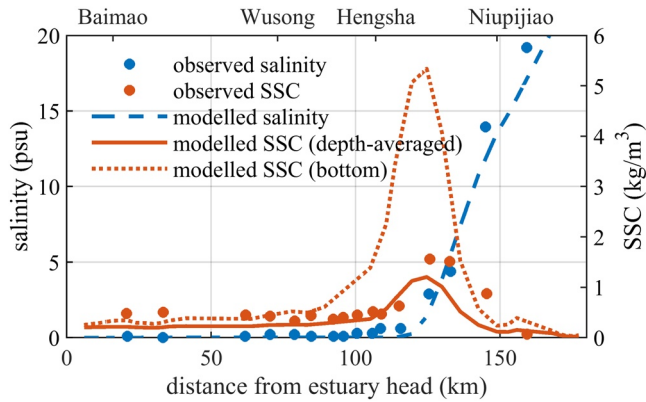
Figure 3. Comparison between modeled (lines) and observed (dots) longitudinal distribution of depth-averaged and bottom suspended sediment concentration (SSC, red) and depth-averaged salinity (blue). The observed data are tidal period and depth-averaged during August 12–16, 2007 from Wan et al., (2014). The modeled salinity and SSC are averaged during the wet season (May-October). The estuary head is at Xuliujing (see Figure 2).

boundaries. The model is run until the computed SSC is in dynamic equilibrium (i.e., the computed SSC remains constant if it is averaged over relevant hydrodynamic timescales such as spring-neap tidal cycles). The modeled ETM is therefore resulting from sediment transport convergence computed by the model, and the strength and location of the ETM are the results of subtle variations in the hydrodynamics. This will be discussed in more detail in Section 4.3. The erosion flux E of cohesive sediment (<64 μm) are calculated with Partheniades-Krone equation (Partheniades, 1965) and deposition D as a bed shear stress independent flux (Winterwerp, 2007):

$$E = M\left(\frac{\tau}{\tau_{cr}} - 1\right), \tag{1}$$

$$D = \alpha\omega_s c, \tag{2}$$

where M is the erosion parameter (kg/m^2/s), τ is the bed shear stress, τ_{cr} is the critical bed shear stress for erosion, ω_s is the settling velocity, c is the SSC, and α is the "reduced deposition" factor used to approximate complex and poorly understood physical processes that occur near the bed and become stronger at high SSC (see van Maren et al., 2020). These processes include hindered settling (reducing the rate at which particles settle on the bed), floc destruction in the bed boundary layer (leading to lower settling velocities), and consolidation (the critical shear stress for erosion is not attained instantaneously, but a particle only gradually gains strength through consolidation after deposition and therefore they are easily immediately re-entrained). All these processes lead to reduced sediment deposition rates at high SSCs. We use a spatially varying α to account for different physical processes which are poorly represented in the model for various reasons. Specifically, $\alpha = 0.1$ is prescribed in the estuary to represent a reduced sediment flux into the bed (resulting from simplification of the consolidation and erosion processes at high concentrations, for instance, as elaborated above), leading to higher near-bottom SSCs; $\alpha = 0$ in the groin field to imply additional sediment availability from the groin field (no deposition, to account for lateral gravity flows and dredging works), and $\alpha = 1$ in the offshore (seaward of the dashed blue line in Figures 1a and 1c) where the majority of sediment supplied to the coastal zone deposits on the inner shelf. The critical shear stresses for erosion is prescribed as 0.1 N/m^2 in the estuary, following earlier sediment transport models developed for the Yangtze Estuary (Chu et al., 2010; Wan & Wang, 2017) and as 0.5 N/m^2 offshore. The small critical shear stress for erosion is characteristic of non-consolidated sediments, which can be easily eroded and re-suspended.

2.2.3. Model Calibration and Scenarios Setup

The model is calibrated in fully baroclinic mode, a standard scenario called Full, which includes both salinity- and sediment-induced density effects (see SI for details). The modeled averaged salinity and SSC show a similar pattern (magnitude and location of the ETM) as observation (Figure 3). The simulated depth-averaged and near-bottom SSC in the ETM reach 1.5 and 5 kg/m^3, respectively, which can sufficiently influence the density of the suspension to reduce vertical mixing rates and corresponding sediment-induced density effects (Winterwerp, 2001). A sensitivity study on the effect of the settling velocity (see SI) reveals that lower settling velocity results in a less pronounced ETM whereas higher settling velocity does not reproduce seasonal variations of SSC. A comparison of the effect of turbulence model parameterizations (see also SI) shows that a k-L turbulence model or additional background vertical viscosity and diffusivity in the k-ε turbulence model could induce more mixing effects, which underestimates the effects of the vertical density gradients on suppressing turbulence. The standard model therefore better represents the seasonal and spatial distributions of the SSC.

We set up four scenarios to investigate the impact of SalDG and SedDG on tidal dynamics and sediment transport (Table 2). Three other scenarios are set up stepwise excluding the SalDG and SedDG, with scenarios defined as Sal (salinity density effect only), Sed (sediment density effect only), and Barot (neither

Table 2
Overview of Model Scenarios

No.	Scenarios	SalDG	SedDG
1	Full*	Yes	Yes
2	Sal	Yes	No
3	Sed	No	Yes
4	Barot	No	No

Note. SalDG, salinity-induced density gradient; SedDG, sediment-induced density gradient. * indicates the fully baroclinic scenario based on which the model is calibrated.

salinity nor sediment density effect, in other words, a barotropic model). Note that the Sal and Barot scenarios exclude the SedDG by excluding the effect of SSC in calculating the density of water (see SI). The differences in the estuarine dynamics between these four scenarios provide the individual effects of salinity and sediment on the ETM.

2.3. Density Parameters

The effect of density differences on hydrodynamics is evaluated by computing the residual flow and the pressure gradient. In the longitudinal momentum equation, the pressure is a function of the barotropic and baroclinic pressure gradient terms:

$$\frac{\partial p}{\partial x} = g \rho_0 \frac{\partial \xi}{\partial x} + g \left(\int_z^\xi \frac{\partial \rho}{\partial x} dz' \right), \tag{3}$$

where x is the along-channel direction, ξ is water surface elevation, ρ_0 is the depth-averaged density, ρ is the density of saltwater containing suspended sediments, g is the gravitational acceleration, and p is the fluid pressure. The first term on the right side is the barotropic pressure gradient and the second term on the right side is the baroclinic pressure gradient F. The baroclinic pressure gradient F, which is estimated from the longitudinal density gradient, is closely related to the residual flow induced by the SalDG and SedDG.

The vertical density effects are expressed using three parameters: The vertical salinity difference, the vertical SSC difference, and the gradient Richardson number. The vertical salinity difference Δs is a simple measure for stratification and is defined as the difference between the bottom and surface salinities ($\Delta s = s_{bottom} - s_{surface}$). Similarly, the vertical SSC difference Δc is obtained from the difference between the bottom and surface SSCs ($\Delta c = c_{bottom} - c_{surface}$). The gradient Richardson number Ri_g is a dimensionless ratio of buoyancy and velocity shear, expressing the stability of the water column:

$$Ri_g = \frac{g(\partial \rho / \partial z)}{\rho (\partial u / \partial z)^2}, \tag{4}$$

where g is the gravitational acceleration. $\partial \rho / \partial z$ and $\partial u / \partial z$ are the vertical gradient of density and horizontal velocity, respectively. Miles (1961) suggest the existence of a critical Ri_g value of 0.25 above which a stable salinity stratification tends to occur, while below which the stratification tends to be unstable and hence tidal mixing is likely to occur. In this work, we calculated the instantaneous Ri_g in which the maximum value over the water column is focused on to indicate the most pronounced changes. The median and interquartile range of the maximum Ri_g over a year in different scenarios are then compared to suggest the changes in stratification.

3. Results

3.1. Tidal Dynamics

The tidal propagation is evaluated by analyzing changes in the M_2 amplitude, M_4 to M_2 amplitude ratio and the phase difference between M_2 and M_4 (Figure 4). The M_2 amplitude landward of 150-km is ~0.08, 0.06 and 0.01 m larger in the Full, Sal and Sed scenarios compared to the Barot

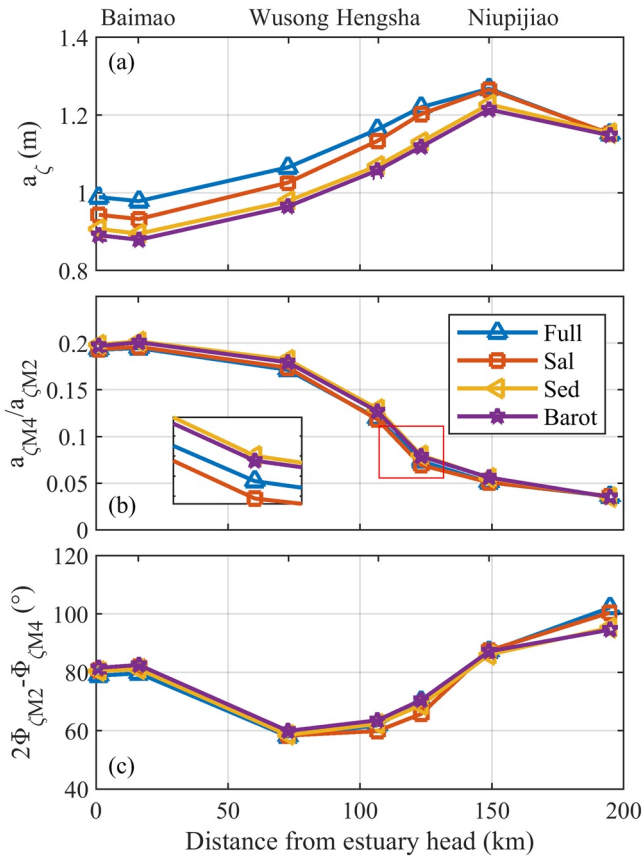**Figure 4.** Modeled longitudinal variations (red dashed line in Figure 2) of (a) water level amplitude M_2 $a_{\zeta M2}$, (b) amplitude ratio of M_4 to M_2 $\left(a_{\zeta M4} / a_{\zeta M2} \right)$ and (c) phase difference between M_2 and M_4 for water levels $(2\phi_{\zeta M2} - \phi_{\zeta M4})$ in scenarios- Full, Sal, Sed, and Barot (see Table 2). The estuary head is at Xuliujing (see also Figure 2).
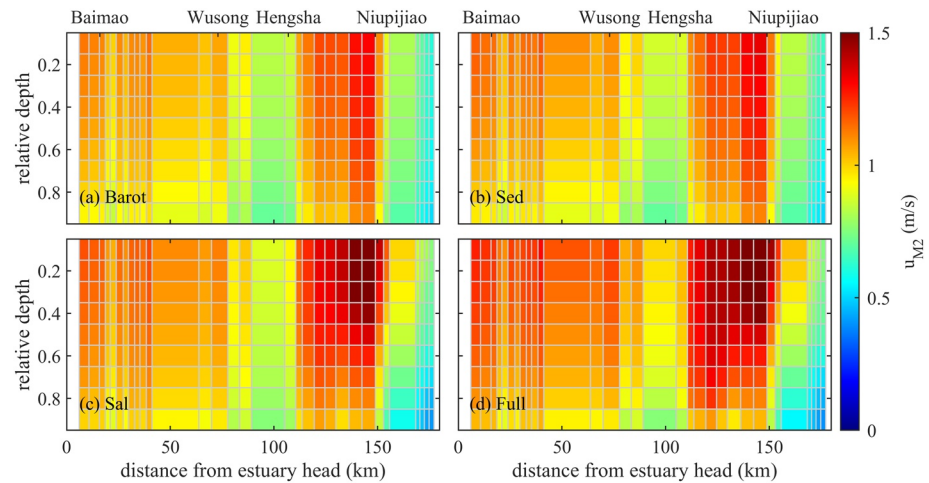
Figure 5. Modeled M_2 amplitude of the longitudinal velocity during a year in the scenarios of (a) Barot, (b) Sed, (c) Sal, and (d) Full (see Table 2). The estuary head is at Xuliujing (see Figure 2).

scenario (representing the combined density effects, and individual SalDG and SedDG effect on tidal amplification, respectively). SalDG (Sal scenario) therefore contributes more to tidal amplification than SedDG (Sed scenario). However, the difference in tidal amplification in the combined scenario (Full scenario) is larger than the sum of the individual effects of SalDG and SedDG, indicating a feedback mechanism between salinity and sediments. Similarly, the effect of SedDG is also stronger on tidal asymmetry (the M_4 to M_2 amplitude ratio and phase difference) when combined with salinity, compared to the individual SedDG (Sed scenario). Specifically, both the amplitude ratio and the phase difference computed with the Sed scenario are very similar to the Barot scenario but strongly differ between the Full and the Sal scenario. It suggests that the effect of the interaction between salinity and sediments is also pronounced in tidal asymmetry. The M_4 to M_2 amplitude ratio and phase difference of scenarios with salinity (Full and Sal) are smaller than in the barotropic scenario (Barot) landward of 150-km (but larger seaward of this point for the phase difference). This suggests that the salinity gradients decrease the degree of tidal wave deformation and behave differently in the regions upstream and downstream of 150-km whereas individual SedDG (Sed scenario) limitedly influences tidal asymmetry. Overall, both SalDG and SedDG lead to slightly larger tidal amplification and deformation; however, the effect of SedDG is only pronounced with the consideration of salinity gradients. It also indicates that salt intrusion, partly as a result of tidal amplification, may be influenced by the effect of SedDG as elaborated later.

The effect of the density gradients on changing flow fields is illustrated with the velocity amplitude of the M_2 tide (Figure 5). The SalDG strongly modifies the flow field, that is, enlarging the flow velocity in the upper water column up to 30% relative to the barotropic scenario (particularly in the ETM), whereas the SedDG does not substantially influence the flow field. This implies that the effect of the SedDG on flow velocities is limited. Again, the differences between the Full and Sal scenarios (representing the effect of sediment in combination) are larger than the effect of sediment alone (the difference between Sed and Barot), allowing us to identify the baroclinic effect of the SedDG in the following sections.

3.2. ETM Location and Extension

The location and extension of the ETM vary in the four scenarios (Figure 6). No significant ETM develops in the Barot scenario, and both surface and bottom along-estuary SSCs are <0.5 kg/m^3 as insufficient sediment trapping mechanisms exist counterbalancing seaward sediment transport by river flow. The Sed scenario exhibits relatively higher bottom SSC at km-90. In the Sal scenario, a significant ETM with maximum bottom SSC <1 kg/m^3 is obtained and the maximum SSC in the ETM occurs between 100 and 150-km which is in agreement with observations (see SI). This suggests the important role of the salinity-induced gravitational circulation on sediment trapping in the Yangtze Estuary. When adding sediment-induced density effects, the near-bottom SSC in the ETM becomes an order of magnitude larger and the extension of the
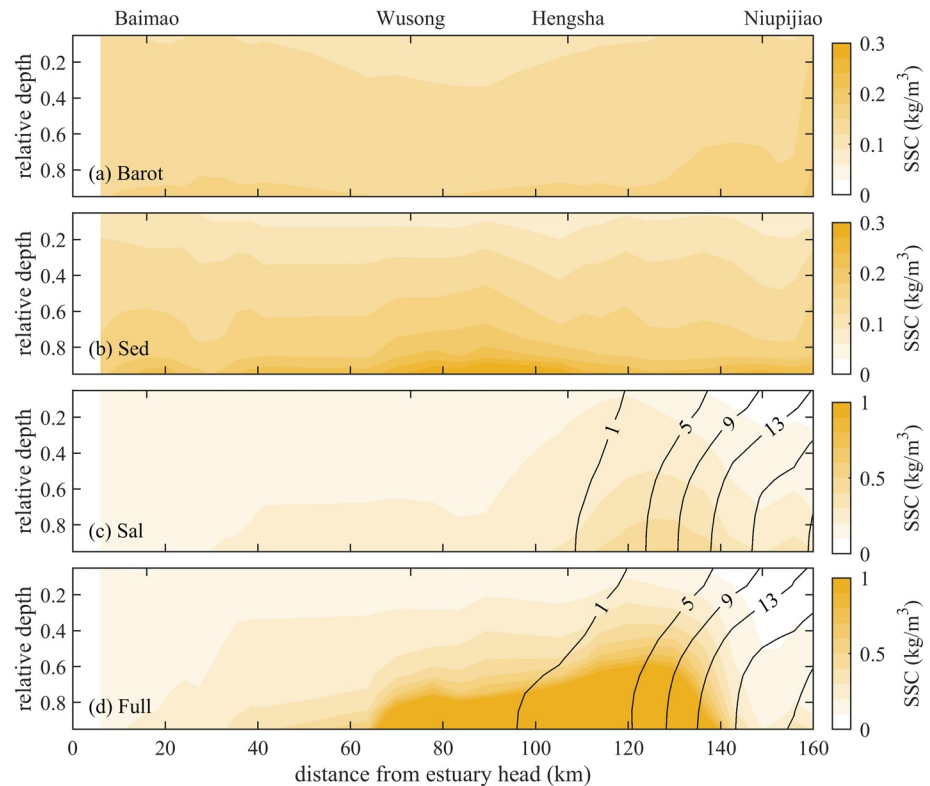
Figure 6. Modeled longitudinal distribution (red dashed line in Figure 2) of salinity (black contour lines) and SSC (color shading) of the scenarios of (a) Barot, (b) Sed, (c) Sal, and (d) Full (see Table 2) averaged from January 1, 2007 to January 1, 2008. The estuary head is at Xuliujing (see also Figure 2). SSC, suspended sediment concentration.

ETM is much wider into the landward side in the Full scenario. The ETM extends further upstream than the observed ETM region identified by Li and Zhang (1998). This longitudinal extent may be the result of the constant settling velocity prescribed in our model whereas in reality the settling velocity is spatially varying, with higher settling velocities in the ETM resulting from salinity effects and high concentrations. Additionally, the salinity is more vertically stratified and the salt front propagates further upstream, i.e., an upstream shift of the near-bed 1 and 5 psu isohalines of ~15 and ~2 km, respectively.

3.3. Density Gradients

3.3.1. Longitudinal Density Gradients

The effects of yearly averaged longitudinal density gradients are analyzed by depicting the longitudinal baroclinic pressure gradient (Figure 7a) and residual current (Figure 8). In the Barot scenario, the longitudinal density gradients are zero as no density effects are considered. In the Sed scenario, the longitudinal density gradients are small and show alternatingly positive and negative values, implying irregularly directed sediment transport. In the Full and Sal scenarios, the baroclinic pressure gradients are always positive seaward of 90-km because of salinity effects, leading to significant landward sediment transport. Interestingly, the baroclinic pressure gradients increase upstream of 120-km and decrease downstream of 120-km in the Full scenario compared with the Sal scenario (interpreted as the effect of sediment in combination with salinity). This suggests that the combined density effects by salt and sediment (Full scenario) are not a sum of the individual effect of the SalDG (Sal scenario) and SedDG (Sed scenario). This is caused by the interaction between salinity and sediments: The distributions of SSC (and therefore the effect of the SedDG) are completely different with and without SalDG (see Figure 6). In other words, when sediment interacts with salinity, the SedDG enhances or strengthens the SalDG in the region landward and seaward of 120-km, respectively. This will be discussed in more detail hereafter.
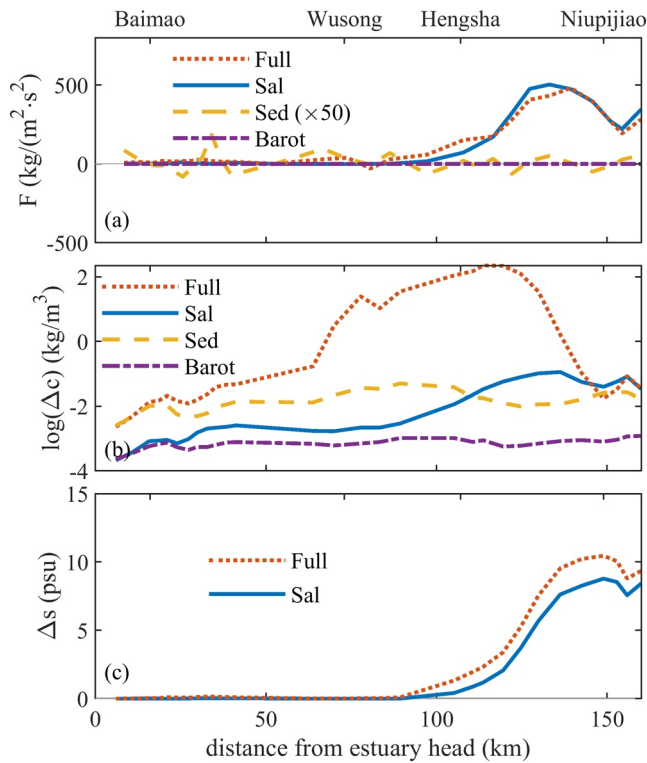
Figure 7. Modeled longitudinal changes (red dashed line in Figure 2) of yearly averaged (a) baroclinic pressure gradient F, (b) vertical suspended sediment concentration (SSC) difference Δ_c (logarithmic scale), and (c) vertical salinity difference Δ_s in the scenarios-Full, Sal, Sed, and Barot (see Table 2). The estuary head is at Xuliujing (see also Figure 2).

Without density effects, the barotropic residual currents are persistently directed seaward due to the large river flow with a magnitude decreasing from 0.4 m/s at 0-km to 0.2 m/s at 150-km (Figure 8a). Therefore, the density-induced residual current patterns are obtained by subtracting the residual current in the Barot scenario from the Sed, Sal, and Full scenarios (Figures 8b–8d). The residual currents induced by SedDG are small and mostly directed seaward except the South Branch landward of km-50 (Figure 8b). Salinity drives a classical residual flow downstream of km-100, with a landward flow (0–0.13 m/s) near the bottom and seaward flow (0–0.23 m/s) near the surface (Figure 8c). Such a residual circulation causes a net landward sediment transport as sediment concentrations are higher near the bed, suggesting that the SalDG is important for the convergence of sediment. Landward of 100-km, the residual current in the deep channel is directed landward (0–0.02 m/s) relative to the barotropic flow in the Sal scenario. This landward flow in the South Channel is compensated by stronger seaward flow in the North Channel (Figures 9a and 9c). Further seaward, in the NP, salinity drives a more classical salinity-induced circulation cell with near-bed inflow and near-surface outflow (Figures 9b and 9d), as also evident in Figure 8c.

Also in the fully baroclinic scenario (Full, also including sediments), a residual circulation exists between 100 and 150-km (Figure 8d). However, the near-surface outflow velocity is ~0.01–0.03 m/s stronger whereas the near-bed inflow increases by 0.01–0.05 m/s (relative to the Sal scenario) between 100 and 140-km. The differences correspond to the changes in surface and bottom residual flow in the South Channel and NP (Figure 9). Moreover, in the South Channel, sediment leads to a reduction of the landward flow in the main channel (as also visible in Figures 8c and 8d) accompanied by more landward flow over shallow areas. This landward flow is compensated by a seaward flow in the North Channel, especially near-surface.

The spatial patterns of residual flow in Figure 9 illustrate that salinity and sediment not only drive the longitudinal and vertical flows but also lateral flows. However, in the remainder of this paper, we will primarily

Figure 8. Modeled longitudinal distribution (red dashed line in Figure 2) of yearly averaged residual currents in the scenarios of the barotropic simulation (a, Barot) and differences of the various baroclinic model runs with the barotropic model (b)–(d). The sediment-only barotropic run is provided in (b) Sed, salinity-only in (c) Sal, and fully baroclinic model in (d) Full (see Table 2) Positive and negative indicates flood (landward) and ebb (seaward) direction, respectively. The estuary head is at Xuliujing (see also Figure 2).

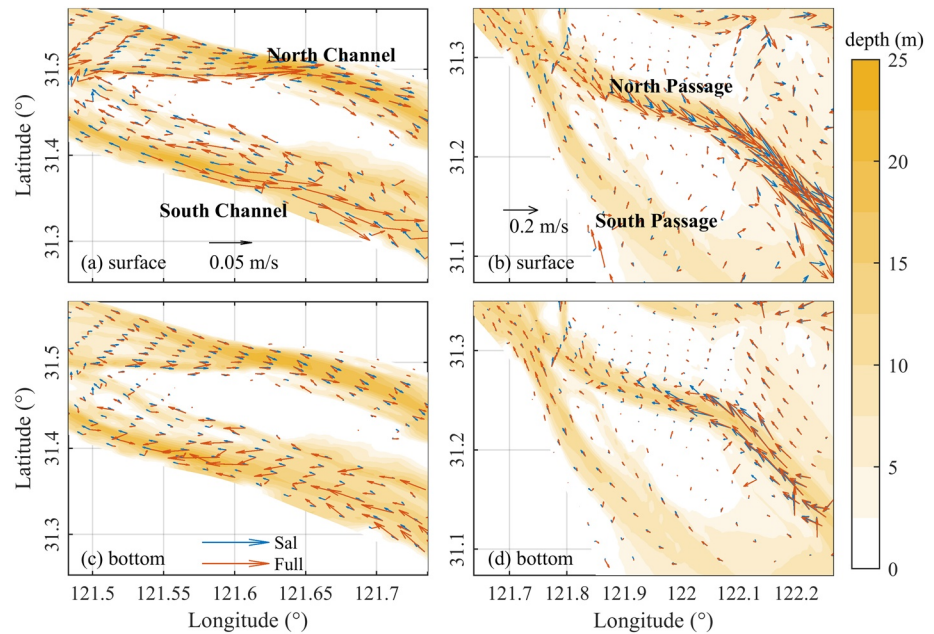**Figure 9.** Comparison of the modeled yearly averaged (a), (b) surface and (c), (d) bottom residual currents (relative to the barotropic model) in the (a), (c) South Channel and (b), (d) North Passage between the Sal and Full scenarios (see Table 2).

address the vertical and longitudinal density effects as we consider these to be the main drivers of sediment transport convergence and divergence which are influenced by sediments. The lateral density effects need to be addressed in greater detail as part of future work.

3.3.2. Vertical Density Gradients

We interpret the vertical density gradients first using the vertical SSC difference (Figure 7b) and the vertical salinity difference (Figure 7c). The vertical SSC difference is smaller than 1 kg/m^3 in all the scenarios except the Full scenario. The maximum vertical SSC difference (0.3 kg/m^3) is at 80-km in the Sed scenario, which may be considered an ETM location resulting from sediment-induced transport processes. On the other hand, the maximum vertical SSC difference (0.4 kg/m^3) locates near the landward limit of the salt wedge in the Sal scenario, corresponding to the role of the SalDG in trapping sediment due to the landward near-bed residual current (see Figure 8c). Similar to the longitudinal density gradients, the effect of SedDG plays an important role only in combination with salinity effects, leading to a pronounced higher near-bed SSC in the Full scenario (in the area in-between the Sal ETM and the Sed ETM). Interestingly, the vertical salinity gradient in the Full scenario is ~1.5 psu larger than that in the Sal scenario downstream of 90-km, suggesting that SedDG strengthens the vertical salinity gradient.
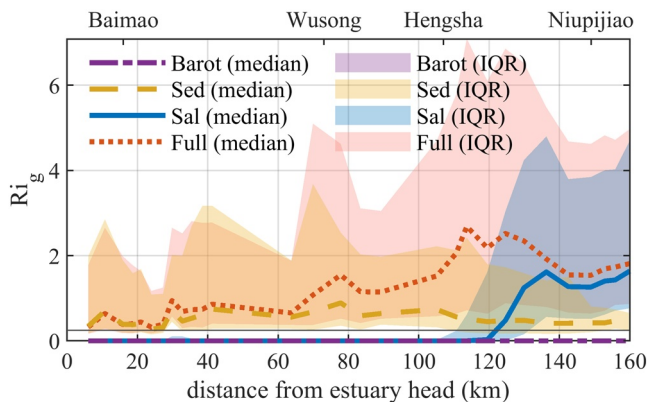

Figure 10. Modeled longitudinal changes (red dashed line in Figure 2) of the median and interquartile range (IQR) of the maximum gradient Richardson number Ri_g over the water column from January 1, 2007 to January 1, 2008 in the scenarios of Barot (purple), Sed (yellow), Sal (blue), and Full (red) (scenarios see Table 2). The values over 0.25 (gray solid line) suggest more stratification effect. The estuary head is at Xuliujing (see also Figure 2).

We subsequently interpret the vertical density gradients with the maximum gradient Richardson number, quantifying the stability of the water column (Figure 10). The water column is stably stratified for $Ri_g > 0.25$, whereas mixing prevails for $Ri_g < 0.25$. The whole channel is stably stratified in the Sed scenario with the largest values upstream of 120-km. Mixing prevails upstream of 120-km in the Sal scenario, but stratified conditions prevail further seaward. The Ri_g in the Full scenario is close to a superposition of the Ri_g values in the Sed and Sal scenarios. However, Ri_g in the Full scenarios is over 2 times stronger than the value in the Sed
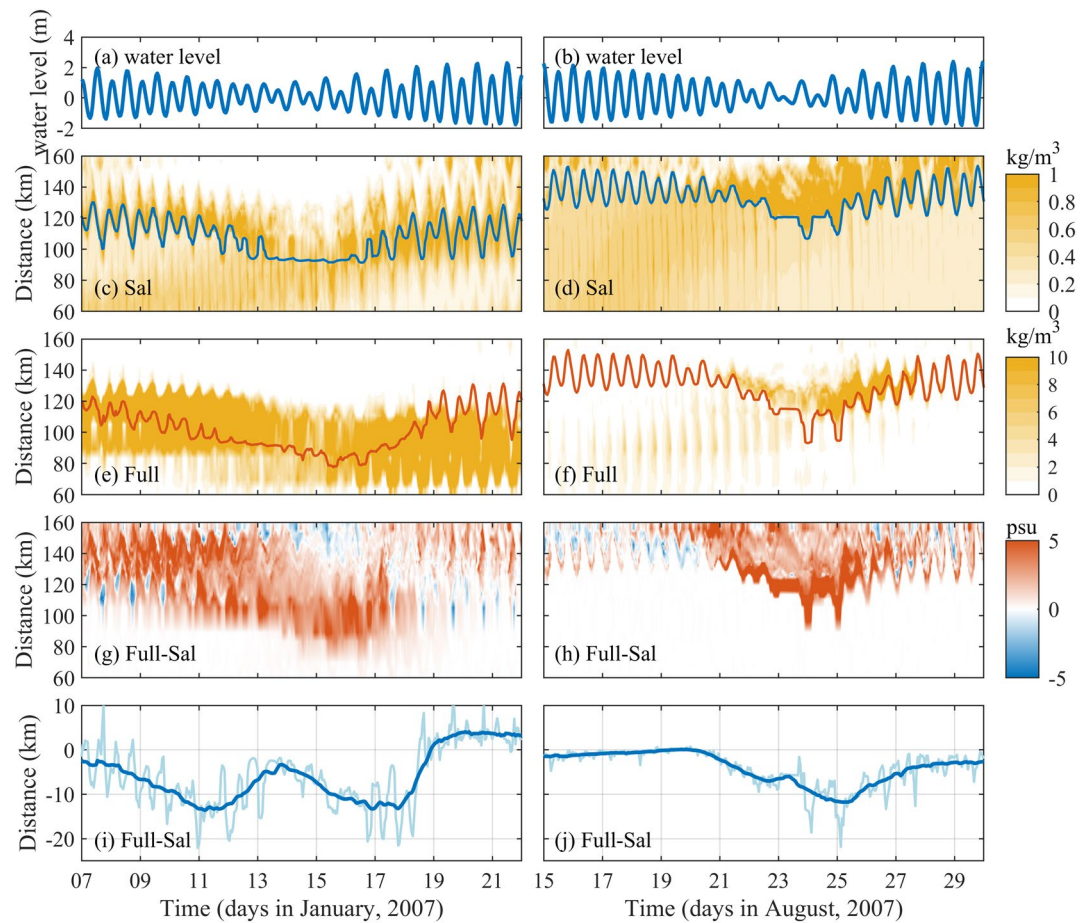
Figure 11. Time evolution of the modeled (a), (b) tidal water level at Niupijiao; bottom suspended sediment concentration (SSC) in the scenarios of (c), (d) Sal, and (e), (f) Full (g), (h) difference of the vertical salinity gradients between the Sal and Full scenarios (Full- Sal) and (i), (j) difference of the instantaneous (thin light blue) and tidally averaged (thick dark blue) salt front locations (Full- Sal) in a spring-neap cycle during (a, c, e, g, i) dry season and (b, d, f, h, j) wet season. The blue and red lines in (c), (d) and (e), (f) represent the tidally averaged salinity front location which is defined as the 3-psu bottom salinity limit, in the Sal and Full scenarios, respectively (scenarios refer to Table 2).

scenario downstream of 60-km and the strongest stratification takes place slightly upstream of the Ri_g peak in the Sal scenario.

3.4. Seasonal and Spring-Neap Variations

The effect of the SedDG on sediment transport and salt intrusion displays strong seasonal and spring-neap variations owing to changes in river discharge and tidal strength (Figure 11). The seasonal variation of the tidal range offshore varies only 10% between the wet and dry season at Niupijiao (see Guo et al., 2015), and therefore the seasonal variability is only evaluated for river discharge. In both the Sal and Full scenarios, the SSC is the largest at intermediate tides during the dry season (Figures 11c and 11e) whereas the SSC is the largest at neap tides during the wet season (Figures 11d and 11f). In the Sal scenario, the location of the maximum SSC in the ETM is more landward in the dry season than in the wet season. Interestingly, the movement of the ETM does not entirely follow the salt front in the Full scenario during the dry season, suggesting an impact of sediment-induced effects on ETM location (superimposed on salinity effects). Furthermore, the SSC in the upper estuary (landward of 100-km) is larger during the wet season than dry season due to the larger sediment input.

The spring-neap variation of the vertical salinity gradient is more pronounced when including sediment-induced density effects, and stronger during the wet season than during the dry season (Figures 11g and 11h). During the wet season, the effect of sediment on salinity gradients is most pronounced during neap tide whereas it is strong at both neap and spring tides during the dry season. This suggests different controlling mechanisms in the dry season compared with the wet season.

The salt front intrudes further landward movement under the influence of SedDG (Figures 11i and 11j), moving up to 20 km landward in the Full scenario compared with the Sal scenario. During the wet season, the salt intrusion moves 5–15 km more landward during neap tides and 0–10 km during spring tides due to the SedDG. During the dry season, the salt intrusion moves farthest landward (10–20 km) at intermediate tides and <5 km (or even seaward) during spring and neap tides due to the SedDG. In addition, the landward movement of the salt wedge due to the SedDG strongly varies with tidal cycles, for instance, the high water and low water can also lead to a maximum of 20 km movement of the salt front induced by the SedDG.

4. Discussion

4.1. Model Limitations

The sediment transport dynamics in the Yangtze Estuary have been extensively studied using numerical models (Chu et al., 2010; Hu et al., 2009; Pang et al., 2010; Song & Wang, 2013). The suspended transport in these models was largely determined by bed erosion and sediment suspension, with highest sediment concentrations occurring in areas with highest flow velocities. This so-called erosion-limited approach (or local sediment source approach, see Brouwer et al., 2018; Dijkstra et al., 2018; van Maren et al., 2020) leads to a strong relation between bed shear stress and turbidity and is less sensitive to variations of residual flows, and therefore altering sediment convergence zones. Instead, we assume that the ETM results from density-driven processes and thus the ETM is more dynamic (supply limited approach, or reduced deposition approach, availability-limited state; see Brouwer et al., 2018; Dijkstra et al., 2018; Hesse et al., 2019; van Maren et al., 2020). The sediment dynamics following a supply limited approach are sensitive to the subtle variations in the hydrodynamic forcing. Using a supply limited approach (as adopted for our study) allows detailed investigations on the formation of the ETM in response to residual sediment transport processes, such as estuarine circulation and tidal asymmetries (Hesse et al., 2019; Van Maren et al., 2011). The supply limited approach has been used in several cases and can result in equilibrium transport for sediment trapping (Brouwer et al., 2018; Dijkstra et al., 2018; Hesse et al., 2019; van Maren, Winterwerp, & Vroom, 2015). One limitation of this approach is the difficulty in calibrating the large-scale model against observations, particularly for the near-bed SSC. Seaward of the NP, the depocenter of the Yangtze subaqueous delta (a ~40 m thick mud belt, Liu et al., 2007), maintains a high deposition rate (10 cm/yr during 1958–2009, Dai et al., 2014) probably as a result of the alongshore current. The simulated ETM formation is also influenced by the deposition zone seaward of the NP (see SI). Moreover, the simulated near-bed SSC and salt intrusion are difficult to be well reproduced simultaneously considering the identified interaction between SSC and salinity; however, it does not negate the main findings in this work.

The modeled depth-averaged SSC corresponds well with data (Figure 3), and the near-bed SSC is substantially larger than averaged over depth (see also Figure 3). However, if we compare the computed near-bed SSC in Figure 3 with an alternative data set (Figure 1), the model seems to underestimate the high concentrations occurring close to the bed (>10 kg/m^3). We attribute this underestimation to (a) flocculation: The settling velocity varies over time and space resulting from flocculation processes influenced by hydrodynamic shear, salinity, and the sediment concentration, which is not numerically accounted for; (b) high SSCs occur as thin layers very close to the bed. The thickness of the near-bed layers is too large (1 m) to resolve such fluid mud layers. These layers result in high SSC concentration gradients, which in turn dampen turbulent mixing, strengthening sediment concentration gradients; (c) consolidation processes are not accounted for which may result in spatially and temporally varying critical bed shear stress. Additionally, the sediment within and seaward of the NP is finer, with lower critical shear stress for erosion. Both consolidation and spatial segregation of sediments may lead to discrepancies of observed and modeled sediment convergence; and (d) The jetties and groins are implemented as blocked thin dams which limit the water and sediment exchanges (Zhu et al., 2017) whereas in reality, the jetties overflow around high water. As a
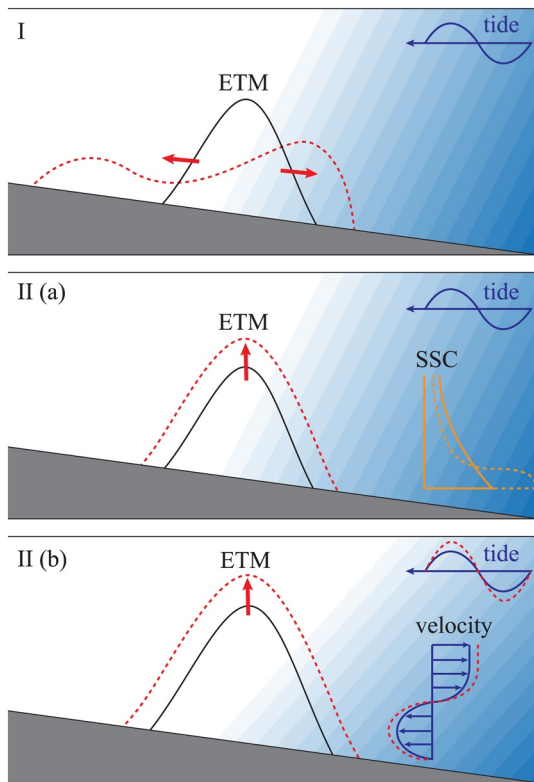
Figure 12. Schematic effects of the longitudinal and vertical sediment-induced density gradients (SedDG) on sediment trapping. I: effect of the longitudinal SedDG; II (a): Effect of the vertical SedDG with changes only in suspended sediment concentration (SSC) (no sediment-induced changes on hydrodynamics); II (b): Effect of the vertical SedDG with changes including hydrodynamics, that is, water level, velocity and salinity. Solid and dashed lines are the situation without and with the effect of the SedDG, respectively.

result, the model underestimates lateral inflow of suspended sediment, especially under high tides and storm events when water levels and SSC are high.

Despite the near-bed SSC underestimation in the ETM, the model does differentiate the effects of longitudinal and vertical SedDG. In reality, the relative effect of the SedDG is expected to be more pronounced, resulting in more pronounced effects on sediment transport and tidal propagation.

4.2. Sediment-Induced Density Effects on ETM Formation

4.2.1. Effect of the SedDG

The effect of the SedDG is completely different with and without salinity effects. Without salinity, no ETM develops and the effect of SedDG is limited. With salinity effects, a pronounced ETM develops with a shape, strength and location strongly influenced by the SedDG. This dependence implies a nonlinear interaction between salinity and SSC, which we address by analyzing the differences between the Sal and Full scenarios. In the following analysis, we differentiate the longitudinal and vertical sediment-induced density effects.

Longitudinal salinity-induced effects trap sediment and therefore generate a pronounced ETM (Figures 6 and 7). In contrast, the longitudinal sediment-induced effects lead to divergence of sediment (I in Figure 12) with sediment transport directed from the middle of the ETM to both the landward and seaward direction. This implies that the longitudinal SedDG strengthens the longitudinal SalDG landward of the ETM, but weakens the longitudinal SalDG seaward of the ETM (corresponding to the increased and decreased baroclinic pressure gradients in the Full scenario compared to the Sal scenario in upstream and downstream of 120-km, respectively, see Figure 7). Therefore, the ETM extends further upstream and the longitudinal distribution of SSC is more asymmetric when accounting for sediment-induced density effects (see Figure 6).

Salinity stratification reduces vertical mixing rates and therefore mitigating tidal damping. This effect is reflected in increasing tidal amplitudes from simulations with salinity (Figure 4). Vertical SedDG influences ETM in two ways. The first (IIa in Figure 12) excludes interaction with the large-scale hydrodynamics (only local turbulent mixing), in which the SedDG increases the vertical concentration gradient (lower surface SSCs and higher bottom SSCs) because of the reduced vertical mixing. These sediment-induced effects become stronger at higher sediment concentrations, leading to progressive sediment trapping in high concentration areas. Even more, strong vertical SSC gradients strengthen the effect of salinity-driven residual circulation on ETM formation. Second, this vertical distribution also influences the large-scale hydrodynamics (water levels, velocities and salinities, see IIb in Figure 12). The vertical SedDG has the same effect as the SalDG on amplifying and deforming tides as vertical density gradients reduce the effective hydraulic drag due to buoyancy destruction (Winterwerp et al., 2009). The drag reduction will subsequently strengthen tidal amplification (Gabioux et al., 2005; Wang et al., 2014; Winterwerp & Wang, 2013) and tidal deformation (van Maren, Winterwerp, & Vroom, 2015). The tides are deformed as friction transfers energy among tidal frequencies and changes the propagation speed at high and low water levels (Friedrichs & Aubrey, 1994; Parker, 1984; Savenije, 2006). More importantly, our work demonstrates that the vertical salinity and sediment effects strengthen each other, introducing a positive feedback mechanism promoting ETM formation.

Overall, this work demonstrates that the longitudinal SedDG leads to sediment transport divergence. This is an important confirmation of the analytical model results of Talke et al. (2009) but also the first time the vertical and longitudinal sediment-induced density effects are differentiated in a complex numerical modeling environment. Particularly the interaction between salinity and SSC indicates that the effect of

the vertical SedDG is even more complicated than mechanisms identified earlier (focusing on the individual contribution of sediment), such as sediment-induced damping of turbulence (Winterwerp, 2001), reduction of hydraulic drag (Winterwerp et al., 2009), and tidal deformation (van Maren, Winterwerp, & Vroom, 2015).

4.2.2. Fluvial and Tidal Effects

The effect of the vertical SedDG is closely related to the seasonal and spring-neap variations of stratification and mixing. Typically, a higher river discharge leads to more stratification compared to a lower discharge, and stronger tidal flow leads to stronger mixing (Dyer, 1986); the river discharge itself leads to tidal damping (Horrevoets et al., 2004) As a result, the SedDG most strongly influences the vertical distribution of the sediment concentration and salinity at neap tides during the wet season, corresponding to the spring-neap variations of the migration of the salt wedge (Figures 11h and 11j). In contrast, in the dry season, the spring-neap variations of the migration of the salt wedge induced by the SedDG are much less related to the enhanced vertical salinity gradients (Figures 11g and 11i). This is probably caused by the spring-neap variation in mixing and deposition which additionally modulates the SSC variation: During the dry season, the near-bed SSC of the salinity-driven ETM (Figures 11c) is smaller at spring tides due to stronger tidal mixing. At neap tides, however, the bottom sediments tend to deposit into the bed, resulting in the lower bottom SSC (as for spring tides, but for a different reason). As a result, vertical SSC differences are low around spring tides and neap tides, but more pronounced in-between.

The strength of the longitudinal SedDG depends on the trapping efficiency as explained above and therefore the expansion of the ETM is most pronounced at intermediate tides during the dry season. Similarly, the strongest effect of the longitudinal SedDG occurs at neap tides during the wet season; however, the divergence of the ETM is not significant. Note that, although the vertical convergence of the ETM is stronger during the wet season than during the dry season, the near-bed SSC is higher during the dry season. Probably, the high river discharge also leads to stronger seaward flushing of sediment, which is more efficiently trapped during the dry season.

4.3. Implications for Other Estuaries

4.3.1. ETM Development

Our work reveals that the SedDG promotes the formation and longitudinal dispersion of the ETM of the Yangtze. These findings are probably relevant for ETM dynamics in other systems as well. ETMs can be classified into three types with respect to their location relative to the salt wedge controlled by different mechanisms (Table 3): Near the landward limit of the salt wedge, far into the freshwater zone, and within the estuarine salinity gradient (Burchard et al., 2018). An ETM may switch location due to river discharges and tide-induced sediment transport. In particular, sediment may play important roles in highly turbid systems. In the Ems estuary, for example, successive channel deepening resulted in the upstream movement of the ETM into the freshwater zone (Chernetsky et al., 2010; de Jonge et al., 2014), which was attributed to positive feedback mechanisms triggered by high SSCs in response to deepening (Dijkstra, Schuttelaars, & Schramkowski, 2019, Dijkstra, Schuttelaars, Schramkowski, & Brouwer, 2019; Winterwerp, 2010; Winterwerp & Wang, 2013; van Maren, Winterwerp, & Vroom, 2015). In addition to these vertical sediment-induced density effects, Talke et al. (2009) suggested longitudinal sediment-induced density effects to generate up-estuary sediment transport in the Ems. In the river-dominated systems, although the ETM is rarely observed to migrate into the freshwater region, ETM dispersion still occurs. For instance, the ETM is weakened from neap tides to spring tides in the Amazon Estuary, which was primarily ascribed to the tidally varying vertical stratification in salinity and sediment (Geyer, 1993). Moreover, the expansion of the ETM is more pronounced in the dry season than the wet season in the Mekong Estuary, which was attributed to the seasonal variation in erosion and deposition processes (Wolanski et al., 1996, 1998). However, the role of sediments in ETM dynamics has received little scientific attention and we believe that the SedDG may be also important for ETM dispersion in other systems.

Table 3
Examples of Estuarine Turbidity Maximums (ETM) With the Main Formation Mechanisms

Type	Main formation mechanisms	Estuaries
ETM1	• topographic trapping (e.g., transition of topography) • under certain conditions (e.g., high river flow)	USA: Chesapeake Bay (Fugate et al., 2007; North & Houde, 2001), Columbia River estuary (Fain et al., 2001; Hudson et al., 2017; Jay & Musiak, 1994), Delaware estuary (Sommerfield & Wong, 2011), Hudson estuary (Geyer et al., 2001; Ralston et al., 2012), San Francisco Bay (Schoellhamer, 2000), York River estuary (Lin & Kuo, 2001)
		Germany: Elbe estuary (Kappenberg & Grabemann, 2001)
		UK: Humber estuary (Mitchell et al., 1998; Uncles et al., 2006)
ETM2	• gravitational circulation (salinity-driven transport)	USA: Chesapeake Bay (Sanford et al., 2001; Schubel, 1968), Columbia River estuary (Jay & Musiak, 1994; Jay & Smith, 1990), Delaware estuary (Sommerfield & Wong, 2011), York River estuary (Lin & Kuo, 2001)
	• tide-induced sediment transport	Germany: Elbe estuary (Postma, 1961), Weser estuary (Grabemann et al., 1997)
		France: Gironde estuary (Allen et al., 1980); Seine estuary (Avoine, 1987; Grasso et al., 2018; Grasso & Le Hir, 2019)
		UK: Humber estuary (Uncles et al., 2006), Tamar estuary (Grabemann et al., 1997)
		Brazil: Amazon Estuary (Geyer, 1993)
		Vietnam: Mekong Estuary (Wolanski et al., 1996, 1998)
		China: Yangtze Estuary (Li et al., 2016; Li and Zhang, 1998; Shi, 2004; Wu et al., 2012)
ETM3	• tide-induced sediment transport • under certain conditions (e.g., low river flow)	Netherlands: Ems estuary (Chernetsky et al., 2010; de Jonge et al., 2014; Talke et al., 2009)
		France: Gironde estuary (Allen et al., 1980; Castaing & Allen, 1981)
		UK: Humber estuary (Mitchell et al., 1998; Uncles et al., 2006), Tamar estuary (Grabemann et al., 1997)

Note. ETM1, ETM2, and ETM3 refer to the ETMs locating within the estuarine salinity gradient, near the landward tip of the salt wedge, and far into the freshwater zone, respectively.
Note: Talke et al., (2009) and this study focuses on the sediment-driven transport in the Ems and the Yangtze Estuary, respectively.

4.4. Salt Intrusion

The landward migration of the salt intrusion induced by SedDG is important for freshwater intake. Approximately 70% of the freshwater supply in Shanghai is taken from the Yangtze Estuary, which is endangered by salinity intrusion (Zhu et al., 2018). Analytical solutions (Cai et al., 2015; Kuijper & Van Rijn, 2011; Savenije, 1993; Zhang et al., 2011) and numerical models (Gong & Shen, 2011; Xue et al., 2009) are often used to predict salt intrusion in estuaries. However, these models do not consider sediment-induced effects on salt intrusion. Our model suggests a 5-km yearly averaged (0–20 km considering seasonal and spring-neap variations) landward movement of the salt intrusion as a result of the SedDG. Note that as our model under-predicts the near-bed SSC, the impact of sediment on salt intrusion may be even larger in reality.

The effect of sediments on salinity is important since the SSC has been changing in many estuaries worldwide. A decrease in riverine sediment flux has been widely reported in many large river deltas due to dam

construction and soil conservation (Syvitski & Saito, 2007; Vörösmarty et al., 2003; Walling, 2009). Although the response time of an estuary to such a riverine sediment decline may be slow (and is often not known), a future decrease in SSC in the estuary may prevent salt intrusion (for instance, resulting from a reduction in river discharge or deepening). However, other estuaries experience an increase in SSC due to local human interventions, such as narrowing and deepening, dredging and dumping activities etc (Winterwerp, 2010, 2013; Winterwerp & Wang, 2013; van Maren, Van Kessel, Cronin, & Sittnoni 2015, van Maren, Winterwerp, & Vroom, 2015). Such an effect, which may be more profound in small estuaries where marine sediment supply dominates the ETMs, could strengthen salt intrusion. Our results on sediment-induced density effects are important for sediment management and management of freshwater supply in turbid estuaries. These findings stress the importance of understanding the effect of human activities within the estuary, in the upstream basin, or through global climate change on estuarine SSC. A change in SSC does not only negatively impact maintenance dredging or estuarine ecology, but also influences salt intrusion through sediment-induced density effects and therefore threatens freshwater availability.

5. Conclusions

Many estuaries are characterized by ETMs generated by salinity-induced density currents and tide-induced transport mechanisms. In this work, we reveal that high sediment concentrations also influence the stability and position of the ETM. The strength and position of ETMs are investigated using a model accounting for the effects of sediment and salinity on longitudinal variations of tidal propagation and sediment transport. Using the Yangtze Estuary as a case study, the model shows that the density effects of salinity and sediment cause ~0.1 m increase in tidal amplitudes. Salinity- and sediment-induced density gradients play different roles in the distribution of SSC along the estuary. Salinity-induced density gradients are the primary drivers for ETM formation leading to the pronounced sediment convergence whereas longitudinal sediment-induced density gradients lead to sediment transport divergence (although depending on the strength of the ETM, which depends on the strength of salinity-driven residual currents). Vertical sediment-induced density gradients introduce a behavior opposite to the longitudinal sediment-induced density gradients on two levels: They (a) enhance the vertical SSC gradients, leading to more efficient salinity-driven residual transport and (b) additionally influence the tidal amplitude, salinity structure, and therefore residual flows, generating a positive feedback mechanism for ETM formation. Summarizing, the strength of the ETM depends on the convergence of the salinity-driven sediment transport, enhanced by the effects of vertical sediment-induced density gradients but weakened by the divergence of sediment resulting from longitudinal sediment-induced density gradients.

We further conclude that sediment-induced density effects vary seasonally and throughout the spring-neap tidal cycles. During the wet season, the vertical salinity gradient is stronger, and therefore the impact of sediment on salt intrusion and ETM formation is more pronounced. The impact is the strongest at neap tides, as during these conditions the water column is more salinity-stratified. During the dry season, in contrast, salt intrusion and ETM displacement are the largest at intermediate tides. This is probably the result of higher near-bed sediment concentrations during that period, resulting from weak vertical mixing while sediment deposition remains limited.

In conclusion, sediment-induced density effects are important for longitudinal tidal propagation, sediment transport, and salt intrusion and should therefore be accounted for in the management of salt intrusion and mitigation of sediment deposition in highly turbid estuaries.

Data Availability Statement

Data in this study are publicly available at https://figshare.com/s/1bf4fa62c006fc3326dc.

References

Allen, G. P., Salomon, J., Bassoullet, P., Du Penhoat, Y., & De Grandpre, C. (1980). Effects of tides on mixing and suspended sediment transport in macrotidal estuaries. *Sedimentary Geology*, *26*(1–3), 69–90. https://doi.org/10.1016/0037-0738(80)90006-8

Avoine, J. (1987). Sediment exchanges between the Seine estuary and its adjacent shelf. *Journal of the Geological Society*, *144*(1), 135–148. https://doi.org/10.1144/gsjgs.144.1.0135

Becker, M., Maushake, C., & Winter, C. (2018). Observations of mud-induced periodic stratification in a hyperturbid estuary. *Geophysical Research Letters*, *45*(11), 5461–5469. https://doi.org/10.1029/2018gl077966

Brenon, I., & Le Hir, P. (1999). Modelling the turbidity maximum in the Seine estuary (France): Identification of formation processes. *Estuarine, Coastal and Shelf Science*, *49*(4), 525–544. https://doi.org/10.1006/ecss.1999.0514

Brouwer, R. L., Schramkowski, G. P., Dijkstra, Y. M., & Schuttelaars, H. M. (2018). Time evolution of estuarine turbidity maxima in well-mixed, tidally dominated estuaries: The role of availability- and erosion-limited conditions. *Journal of Physical Oceanography*, *48*(8), 1629–1650. https://doi.org/10.1175/jpo-d-17-0183.1

Burchard, H., & Baumert, H. (1998). The formation of estuarine turbidity maxima due to density effects in the salt wedge. A hydrodynamic process study. *Journal of Physical Oceanography*, *28*(2), 309–321. https://doi.org/10.1175/1520-0485(1998)028<0309:tfoetm>2.0.co;2

Burchard, H., Schuttelaars, H. M., & Ralston, D. K. (2018). Sediment trapping in estuaries. *Annual Review of Marine Science*, *10*, 371–395. https://doi.org/10.1146/annurev-marine-010816-060535

Cai, H., Savenije, H. H. G., Zuo, S., Jiang, C., & Chua, V. P. (2015). A predictive model for salt intrusion in estuaries applied to the Yangtze estuary. *Journal of Hydrology*, *529*, 1336–1349. https://doi.org/10.1016/j.jhydrol.2015.08.050

Castaing, P., & Allen, G. P. (1981). Mechanisms controlling seaward escape of suspended sediment from the Gironde: A macrotidal estuary in France. *Marine Geology*, *40*(1–2), 101–118. https://doi.org/10.1016/0025-3227(81)90045-1

Chernetsky, A. S., Schuttelaars, H. M., & Talke, S. A. (2010). The effect of tidal asymmetry and temporal settling lag on sediment trapping in tidal estuaries. *Ocean Dynamics*, *60*(5), 1219–1241. https://doi.org/10.1007/s10236-010-0329-8

Chu, A., Wang, Z., De Vriend, H., & Stive, M. (2010). A process-based approach to sediment transport in the Yangtze Estuary. Paper presented at 32nd International Conference on Coastal Engineering. Shanghai, China. ICCE.

Dai, Z., Liu, J. T., Wei, W., & Chen, J. (2014). Detection of the three Gorges dam influence on the Changjiang (Yangtze river) submerged delta. *Scientific Reports*, *4*, 6600. https://doi.org/10.1038/srep06600

de Jonge, V. N., Schuttelaars, H. M., van Beusekom, J. E. E., Talke, S. A., & de Swart, H. E. (2014). The influence of channel deepening on estuarine turbidity levels and dynamics, as exemplified by the Ems estuary. *Estuarine, Coastal and Shelf Science*, *139*, 46–59. https://doi.org/10.1016/j.ecss.2013.12.030

Dijkstra, Y. M., Schuttelaars, H. M., & Schramkowski, G. P. (2019). A regime shift from low to high sediment concentrations in a tide-dominated estuary. *Geophysical Research Letters*, *46*(8), 4338–4345. https://doi.org/10.1029/2019gl082302

Dijkstra, Y. M., Schuttelaars, H. M., Schramkowski, G. P., & Brouwer, R. L. (2019). Modeling the transition to high sediment concentrations as a response to channel deepening in the Ems River Estuary. *Journal of Geophysical Research: Oceans*, *124*(3), 1578–1594. https://doi.org/10.1029/2018jc014367

Dijkstra, Y. M., Schuttelaars, H. M., & Winterwerp, J. C. (2018). The hyperturbid state of the water column in estuaries and rivers: The importance of hindered settling. *Ocean Dynamics*, *68*(3), 377–389. https://doi.org/10.1007/s10236-018-1132-1

Doxaran, D., Froidefond, J.-M., Castaing, P., & Babin, M. (2009). Dynamics of the turbidity maximum zone in a macrotidal estuary (the Gironde, France): Observations from field and MODIS satellite data. *Estuarine, Coastal and Shelf Science*, *81*(3), 321–332. https://doi.org/10.1016/j.ecss.2008.11.013

Dyer, K. (1986). *Coastal and estuarine sediment dynamics* (p. 358). Chichester: John Wiley and Sons.

Dyer, K. R. (1988). Fine sediment particle transport in estuaries. In Physical processes in estuaries (pp. 295–310). Springer. https://doi.org/10.1007/978-3-642-73691-9_16

Egbert, G. D., Bennett, A. F., & Foreman, M. G. G. (1994). TOPEX/POSEIDON tides estimated using a global inverse model. *Journal of Geophysical Research*, *99*(C12), 24821–24852. https://doi.org/10.1029/94jc01894

Egbert, G. D., & Erofeeva, S. Y. (2002). Efficient inverse modeling of barotropic ocean tides. *Journal of Atmospheric and Oceanic Technology*, *19*(2), 183–204. https://doi.org/10.1175/1520-0426(2002)019<0183:eimobo>2.0.co;2

Fain, A. M. V., Jay, D. A., Wilson, D. J., Orton, P. M., & Baptista, A. M. (2001). Seasonal and tidal monthly patterns of particulate matter dynamics in the Columbia River estuary. *Estuaries*, *24*(5), 770–786. https://doi.org/10.2307/1352884

Festa, J. F., & Hansen, D. V. (1978). Turbidity maxima in partially mixed estuaries: A two-dimensional numerical model. *Estuarine and Coastal Marine Science*, *7*(4), 347–359. https://doi.org/10.1016/0302-3524(78)90087-7

Friedrichs, C. T., & Aubrey, D. G. (1988). Non-linear tidal distortion in shallow well-mixed estuaries: A synthesis. *Estuarine, Coastal and Shelf Science*, *27*(5), 521–545. https://doi.org/10.1016/0272-7714(88)90082-0

Friedrichs, C. T., & Aubrey, D. G. (1994). Tidal propagation in strongly convergent channels. *Journal of Geophysical Research*, *99*(C2), 3321. https://doi.org/10.1029/93jc03219

Fugate, D. C., Friedrichs, C. T. and Sanford, L. P. (2007). Lateral dynamics and associated transport of sediment in the upper reaches of a partially mixed estuary, Chesapeake Bay, USA. *Continental Shelf Research*, *27*(5), 679–698. https://doi.org/10.1016/j.csr.2006.11.012

Gabioux, M., Vinzon, S. B., & Paiva, A. M. (2005). Tidal propagation over fluid mud layers on the Amazon shelf. *Continental Shelf Research*, *25*(1), 113–125. https://doi.org/10.1016/j.csr.2004.09.001

Geyer, W. R. (1993). The importance of suppression of turbulence by stratification on the estuarine turbidity maximum. *Estuaries*, *16*(1), 113–125. https://doi.org/10.2307/1352769

Geyer, W. R., & MacCready, P. (2014). The estuarine circulation. *Annual Review of Fluid Mechanics*, *46*(1), 175–197. https://doi.org/10.1146/annurev-fluid-010313-141302

Geyer, W. R., Woodruff, J. D., & Traykovski, P. (2001). Sediment transport and trapping in the Hudson River estuary. *Estuaries*, *24*(5), 670–679. https://doi.org/10.2307/1352875

Gong, W., & Shen, J. (2011). The response of salt intrusion to changes in river discharge and tidal mixing during the dry season in the Modaomen Estuary, China. *Continental Shelf Research*, *31*(7–8), 769–788. https://doi.org/10.1016/j.csr.2011.01.011

Grabemann, I., Uncles, R. J., Krause, G., & Stephens, J. A. (1997). Behaviour of turbidity maxima in the Tamar (U.K.) and Weser (F.R.G.) estuaries. *Estuarine, Coastal and Shelf Science*, *45*(2), 235–246. https://doi.org/10.1006/ecss.1996.0178

Grasso, F., & Le Hir, P. (2019). Influence of morphological changes on suspended sediment dynamics in a macrotidal estuary: Diachronic analysis in the Seine estuary (France) from 1960 to 2010. *Ocean Dynamics*, *69*(1), 83–100. https://doi.org/10.1007/s10236-018-1233-x

Grasso, F., Verney, R., Le Hir, P., Thouvenin, B., Schulz, E., Kervella, Y., et al. (2018). Suspended sediment dynamics in the macrotidal Seine estuary (France): 1. Numerical modeling of turbidity maximum dynamics. *Journal of Geophysical Research: Oceans*, *123*(1), 558–577. https://doi.org/10.1002/2017jc013185

Guo, L., & He, Q. (2011). Freshwater flocculation of suspended sediments in the Yangtze River, China. *Ocean Dynamics*, *61*(2–3), 371–386. https://doi.org/10.1007/s10236-011-0391-x

Guo, L., van der Wegen, M., Jay, D. A., Matte, P., Wang, Z. B., Roelvink, D., & He, Q. (2015). River-tide dynamics: Exploration of nonstationary and nonlinear tidal behavior in the Yangtze River estuary. *Journal of Geophysical Research: Oceans*, *120*(5), 3499–3521. https://doi.org/10.1002/2014jc010491

Hesse, R. F., Zorndt, A., & Fröhle, P. (2019). Modelling dynamics of the estuarine turbidity maximum and local net deposition. *Ocean Dynamics*, *69*(4), 489–507. https://doi.org/10.1007/s10236-019-01250-w

Horrevoets, A. C., Savenije, H. H. G., Schuurman, J. N., & Graas, S. (2004). The influence of river discharge on tidal damping in alluvial estuaries. *Journal of Hydrology*, *294*(4), 213–228. https://doi.org/10.1016/j.jhydrol.2004.02.012

Hu, K., Ding, P., Wang, Z., & Yang, S. (2009). A 2D/3D hydrodynamic and sediment transport model for the Yangtze Estuary, China. *Journal of Marine Systems*, *77*(1–2), 114–136. https://doi.org/10.1016/j.jmarsys.2008.11.014

Hu, K. L., Ding, P. X., Zhu, S. X., & Cao, Z. Y. (2000). 2-D current field numerical simulation integrating Yangtze Estuary with Hangzhou Bay. *China Ocean Engineering*, *14*(1), 89–102.

Hudson, A. S., Talke, S. A., & Jay, D. A. (2017). Using satellite observations to characterize the response of estuarine turbidity maxima to external forcing. *Estuaries and Coasts*, *40*(2), 343–358. https://doi.org/10.1007/s12237-016-0164-3

Jay, D. A., & Musiak, J. D. (1994). Particle trapping in estuarine tidal flows. *Journal of Geophysical Research*, *99*(C10), 20445. https://doi.org/10.1029/94jc00971

Jay, D. A., & Musiak, J. D. (1996).Internal tidal asymmetry in channel flows: Origins and consequences. *Coastal and Estuarine Studies*, *50*, 211–249. https://doi.org/10.1029/CE050p0211

Jay, D. A., & Smith, J. D. (1990). Circulation, density distribution and neap-spring transitions in the Columbia River Estuary. *Progress in Oceanography*, *25*(1–4), 81–112. https://doi.org/10.1016/0079-6611(90)90004-l

Jiang, C., de Swart, H. E., Li, J., & Liu, G. (2013). Mechanisms of along-channel sediment transport in the North Passage of the Yangtze Estuary and their response to large-scale interventions. *Ocean Dynamics*, *63*(2–3), 283–305. https://doi.org/10.1007/s10236-013-0594-4

Jiang, X., Lu, B., & He, Y. (2013). Response of the turbidity maximum zone to fluctuations in sediment discharge from river to estuary in the Changjiang Estuary (China). *Estuarine, Coastal and Shelf Science*, *131*, 24–30. https://doi.org/10.1016/j.ecss.2013.07.003

Kappenberg, J., & Grabemann, I. (2001). Variability of the mixing zones and estuarine turbidity maxima in the Elbe and Weser estuaries. *Estuaries*, *24*(5), 699–706. https://doi.org/10.2307/1352878

Kuang, C.-P., Chen, W., Gu, J., & He, L.-L. (2014). Comprehensive analysis on the sediment siltation in the upper reach of the Deepwater navigation channel in the Yangtze Estuary. *Journal of Hydrodynamics*, *26*(2), 299–308. https://doi.org/10.1016/s1001-6058(14)60033-0

Kuijper, K., & Van Rijn, L. C. (2011). Analytical and numerical analysis of tides and salinities in estuaries; Part II: Salinity distributions in prismatic and convergent tidal channels. *Ocean Dynamics*, *61*(11), 1743–1765. https://doi.org/10.1007/s10236-011-0454-z

Lesser, G. R., Roelvink, J. A., van Kester, J. A. T. M., & Stelling, G. S. (2004). Development and validation of a three-dimensional morphological model. *Coastal Engineering*, *51*(8–9), 883–915. https://doi.org/10.1016/j.coastaleng.2004.07.014

Li, J. F. & Zhang, C. (1998), Sediment resuspension and implications for turbidity maximum in the Changjiang estuary. *Marine Geology*, *148*(3–4), 117–124. https://doi.org/10.1016/S0025-3227(98)00003-6

Li, L., He, Z., Xia, Y., & Dou, X. (2018). Dynamics of sediment transport and stratification in Changjiang River Estuary, China. *Estuarine, Coastal and Shelf Science*, *213*, 1–17. https://doi.org/10.1016/j.ecss.2018.08.002

Li, X., Zhu, J., Yuan, R., Qiu, C., & Wu, H. (2016). Sediment trapping in the Changjiang Estuary: Observations in the north passage over a spring-neap tidal cycle. *Estuarine, Coastal and Shelf Science*, *177*, 8–19. https://doi.org/10.1016/j.ecss.2016.05.004

Lin, J., He, Q., Guo, L., van Prooijen, B. C., & Wang, Z. B. (2019). An integrated optic and acoustic (IOA) approach for measuring suspended sediment concentration in highly turbid environments. *Marine Geology*, *421*, 106062.

Lin, J., & Kuo, A. Y. (2001). Secondary turbidity maximum in a partially mixed microtidal estuary. *Estuaries*, *24*(5), 707–720. https://doi.org/10.2307/1352879

Liu, G., Zhu, J., Wang, Y., Wu, H., & Wu, J. (2011). Tripod measured residual currents and sediment flux: Impacts on the silting of the Deepwater navigation channel in the Changjiang Estuary. *Estuarine, Coastal and Shelf Science*, *93*(3), 192–201. https://doi.org/10.1016/j.ecss.2010.08.008

Liu, J. P., Xu, K. H., Li, A. C., Milliman, J. D., Velozzi, D. M., Xiao, S. B., & Yang, Z. S. (2007). Flux and fate of Yangtze River sediment delivered to the East China Sea. *Geomorphology*, *85*(3–4), 208–224. https://doi.org/10.1016/j.geomorph.2006.03.023

MacCready, P., & Geyer, W. R. (2010). Advances in estuarine physics. *Annual Review Marine Science*, *2*, 35–58. https://doi.org/10.1146/annurev-marine-120308-081015

Miles, J. W. (1961). On the stability of heterogeneous shear flows. *Journal of Fluid Mechanics*, *10*(4), 496–508. https://doi.org/10.1017/s0022112061000305

Mitchell, S., West, J., Arundale, A., Guymer, I., & Couperthwaite, J. (1998). Dynamics of the turbidity maxima in the upper Humber estuary system, UK. *Marine Pollution Bulletin*, *37*(3–7), 190–205.

North, E. W., & Houde, E. D. (2001). Retention of white perch and striped bass larvae: Biological-physical interactions in Chesapeake Bay estuarine turbidity maximum. *Estuaries*, *24*(5), 756–769. https://doi.org/10.2307/1352883

Pang, C., Zhao, E., & Yang, Y. (2010). Numerical simulation on the process of saltwater intrusion and its impact on the suspended sediment concentration in the Changjiang (Yangtze) estuary. *Chinese Journal of Oceanology and Limnology*, *28*(3), 609–619. https://doi.org/10.1007/s00343-010-9254-4

Parker, B. B. (1984). *Frictional effects on the tidal dynamics of a shallow estuary*.

Partheniades, E. (1965). Erosion and deposition of cohesive soils. *Journal of the Hydraulics Division*, *91*(1), 105–139. https://doi.org/10.1061/jyceaj.0001165

Postma, H. (1961). Transport and accumulation of suspended matter in the Dutch Wadden Sea. *Netherlands Journal of Sea Research*, *1*(1–2), 148–190. https://doi.org/10.1016/0077-7579(61)90004-7

Pu, X., Shi, J. Z., Hu, G.-D., & Xiong, L.-B. (2015). Circulation and mixing along the north passage in the Changjiang river estuary, China. *Journal of Marine Systems*, *148*, 213–235. https://doi.org/10.1016/j.jmarsys.2015.03.009

Ralston, D. K., Geyer, W. R., & Warner, J. C. (2012). Bathymetric controls on sediment transport in the Hudson river estuary: Lateral asymmetry and frontal trapping. *Journal of Geophysical Research*, *117*(C10). https://doi.org/10.1029/2012jc008124

Sanford, L. P., Suttles, S. E., & Halka, J. P. (2001). Reconsidering the physics of the Chesapeake Bay estuarine turbidity maximum. *Estuaries*, *24*(5), 655–669. https://doi.org/10.2307/1352874

Savenije, H. H. (1993). Predictive model for salt intrusion in estuaries. *Journal of Hydrology*, *148*(1–4), 203–218. https://doi.org/10.1016/0022-1694(93)90260-g

Savenije, H. H. (2006). *Salinity and tides in alluvial estuaries*. Elsevier.

Schoellhamer, D. H. (2000). Influence of salinity, bottom topography, and tides on locations of estuarine turbidity maxima in northern San Francisco Bay. In *Proceedings in Marine Science* (pp. 343–357). Elsevier. https://doi.org/10.1016/s1568-2692(00)80130-8

Schubel, J. R. (1968). Turbidity maximum of the northern Chesapeake bay. *Science*, *161*(3845), 1013–1015. https://doi.org/10.1126/science.161.3845.1013

Shi, Z. (2004). Behaviour of fine suspended sediment at the north passage of the Changjiang estuary, China. *Journal of Hydrology*, *293*(1–4), 180–190. https://doi.org/10.1016/j.jhydrol.2004.01.014

Simpson, J. H., Brown, J. Matthews, J., & Allen, G. (1990). Tidal straining, density currents, and stirring in the control of estuarine Stratification. *Estuaries*, *13*(2), 125–132. https://doi.org/10.2307/1351581

Sommerfield, C. K., & Wong, K.-C. (2011). Mechanisms of sediment flux and turbidity maintenance in the Delaware Estuary. *Journal of Geophysical Research*, *116*(C1). https://doi.org/10.1029/2010jc006462

Song, D., & Wang, X. H. (2013). Suspended sediment transport in the Deepwater navigation Channel, Yangtze River Estuary, China, in the dry season 2009: 2. Numerical simulations. *Journal of Geophysical Research: Oceans*, *118*(10), 5568–5590. https://doi.org/10.1002/jgrc.20411

Song, D., Wang, X. H., Cao, Z., & Guan, W. (2013). Suspended sediment transport in the Deepwater navigation channel, Yangtze river estuary, China, in the dry season 2009: 1. Observations over spring and neap tidal cycles. *Journal of Geophysical Research: Oceans*, *118*(10), 5555–5567. https://doi.org/10.1002/jgrc.20410

Syvitski, J. P., & Saito, Y. (2007). Morphodynamics of deltas under the influence of humans. *Global and Planetary Change*, *57*(3–4), 261–282. https://doi.org/10.1016/j.gloplacha.2006.12.001

Talke, S. A., de Swart, H. E., & Schuttelaars, H. M. (2009). Feedback between residual circulations and sediment distribution in highly turbid estuaries: An analytical model. *Continental Shelf Research*, *29*(1), 119–135. https://doi.org/10.1016/j.csr.2007.09.002

Talke, S. A., & Jay, D. A. (2020). Changing tides: The role of natural and anthropogenic factors. *Annual Review Marine Science*, *12*, 121–151. https://doi.org/10.1146/annurev-marine-010419-010727

Uncles, R., Stephens, J., & Harris, C. (2006). Runoff and tidal influences on the estuarine turbidity maximum of a highly turbid system: The upper Humber and Ouse Estuary, UK. *Marine Geology*, *235*(1–4), 213–228. https://doi.org/10.1016/j.margeo.2006.10.015

Uncles, R. J., Elliott, R. C. A., & Weston, S. A. (1985). Observed fluxes of water, salt and suspended sediment in a partly mixed estuary. *Estuarine, Coastal and Shelf Science*, *20*(2), 147–167. https://doi.org/10.1016/0272-7714(85)90035-6

van Maren, D., Vroom, J., Fettweis, M., & Vanlede, J. (2020). Formation of the Zeebrugge coastal turbidity maximum: The role of uncertainty in near-bed exchange processes. *Marine Geology*, *425*, 106186.

van Maren, D. S., van Kessel, T., Cronin, K., & Sittoni, L. (2015). The impact of channel deepening and dredging on estuarine sediment concentration. *Continental Shelf Research*, *95*, 1–14. https://doi.org/10.1016/j.csr.2014.12.010

Van Maren, D. S., Winterwerp, J. C., Decrop, B., Wang, Z. B., & Vanlede, J. (2011). Predicting the effect of a current deflecting wall on harbour siltation. *Continental Shelf Research*, *31*(10), S182–S198. https://doi.org/10.1016/j.csr.2010.12.005

van Maren, D. S., Winterwerp, J. C., & Vroom, J. (2015). Fine sediment transport into the hyper-turbid lower Ems River: The role of channel deepening and sediment-induced drag reduction. *Ocean Dynamics*, *65*(4), 589–605. https://doi.org/10.1007/s10236-015-0821-2

Vörösmarty, C. J., Meybeck, M., Fekete, B., Sharma, K., Green, P., & Syvitski, J. P. M. (2003). Anthropogenic sediment retention: Major global impact from registered river impoundments. *Global and Planetary Change*, *39*(1–2), 169–190. https://doi.org/10.1016/s0921-8181(03)00023-7

Walling, D. E. (2009). *The impact of global change on erosion and sediment transport by rivers: Current progress and future challenges*. Unesco.

Wan, Y., Gu, F., Wu, H., & Roelvink, D. (2014). Hydrodynamic evolutions at the Yangtze Estuary from 1998 to 2009. *Applied Ocean Research*, *47*, 291–302. https://doi.org/10.1016/j.apor.2014.06.009

Wan, Y., & Wang, L. (2017). Numerical investigation of the factors influencing the vertical profiles of current, salinity, and SSC within a turbidity maximum zone. *International Journal of Sediment Research*, *32*(1), 20–33. https://doi.org/10.1016/j.ijsrc.2016.07.003

Wang, Z. B., Winterwerp, J. C., & He, Q. (2014). Interaction between suspended sediment and tidal amplification in the Guadalquivir Estuary. *Ocean Dynamics*, *64*(10), 1487–1498. https://doi.org/10.1007/s10236-014-0758-x

Winterwerp, J. C. (2001). Stratification effects by cohesive and noncohesive sediment. *Journal of Geophysical Research*, *106*(C10), 22559–22574. https://doi.org/10.1029/2000jc000435

Winterwerp, J. C. (2007). On the sedimentation rate of cohesive sediment. *Proceedings in Marine Science*, *8*, 209–226. https://doi.org/10.1016/s1568-2692(07)80014-3

Winterwerp, J. C. (2010). Fine sediment transport by tidal asymmetry in the high-concentrated Ems River: Indications for a regime shift in response to channel deepening. *Ocean Dynamics*, *61*(2–3), 203–215. https://doi.org/10.1007/s10236-010-0332-0

Winterwerp, J. C., Lely, M., & He, Q. (2009). Sediment-induced buoyancy destruction and drag reduction in estuaries. *Ocean Dynamics*, *59*(5), 781–791. https://doi.org/10.1007/s10236-009-0237-y

Winterwerp, J. C., & Wang, Z. B. (2013). Man-induced regime shifts in small estuaries-I: Theory. *Ocean Dynamics*, *63*(11–12), 1279–1292. https://doi.org/10.1007/s10236-013-0662-9

Winterwerp, J. C., Wang, Z. B., van Braeckel, A., van Holland, G., & Kösters, F. (2013). Man-induced regime shifts in small estuaries-II: A comparison of rivers. *Ocean Dynamics*, *63*(11–12), 1293–1306. https://doi.org/10.1007/s10236-013-0663-8

Wolanski, E., Ngoc Huan, N., Trong Dao, L., Huu Nhan, N., & Ngoc Thuy, N. (1996), Fine-sediment dynamics in the Mekong river estuary, Vietnam. *Estuarine, Coastal and Shelf Science*, *43*(5), 565–582. https://doi.org/10.1006/ecss.1996.0088

Wolanski, E., Nhan, N. H., & Spagnol, S. (1998). Sediment dynamics during low flow conditions in the Mekong river estuary, Vietnam. *Journal of Coastal Research*, 472–482.

Wu, J., Liu, J. T., & Wang, X. (2012). Sediment trapping of turbidity maxima in the Changjiang Estuary. *Marine Geology*, *303–306*, 14–25. https://doi.org/10.1016/j.margeo.2012.02.011

Xue, P., Chen, C., Ding, P., Beardsley, R. C., Lin, H., Ge, J., & Kong, Y. (2009). Saltwater intrusion into the Changjiang River: A model-guided mechanism study. *Journal of Geophysical Research*, *114*(C2). https://doi.org/10.1029/2008jc004831

Yu, Q., Wang, Y., Gao, J., Gao, S., & Flemming, B. (2014). Turbidity maximum formation in a well-mixed macrotidal estuary: The role of tidal pumping. *Journal of Geophysical Research: Oceans*, *119*(11), 7705–7724. https://doi.org/10.1002/2014jc010228

Yun, C. (2004). *Recent development of the Changjiang estuary* (p. 320). Beijing: China Ocean Press.

Zhang, E., Savenije, H. H. G., Wu, H., Kong, Y., & Zhu, J. (2011). Analytical solution for salt intrusion in the Yangtze Estuary, China. *Estuarine, Coastal and Shelf Science*, *91*(4), 492–501. https://doi.org/10.1016/j.ecss.2010.11.008

Zhu, C., Guo, L., van Maren, D., Tian, B., Wang, X., He, Q., & Wang, Z. B. (2019). Decadal morphological evolution of the mouth zone of the Yangtze Estuary in response to human interventions. *Earth Surface Processes and Landforms*, *44*(12), 2319–2332.

Zhu, L., He, Q., & Shen, J. (2017). Modeling lateral circulation and its influence on the along-channel flow in a branched estuary. *Ocean Dynamics*, *68*(2), 177–191. https://doi.org/10.1007/s10236-017-1114-8

Zhu, L., He, Q., Shen, J., Qiu, C., IntechOpen, L., He, Q., & Shen, J. (2018). Modeling lateral circulation and its influence on the along-channel flow in a branched estuary. In *Coastal Environment, disaster, and infrastructure-A Case study of China's coastline*.

Zhu, L., He, Q., Shen, J., & Wang, Y. (2016). The influence of human activities on morphodynamics and alteration of sediment source and sink in the Changjiang estuary. *Geomorphology*, *273*, 52–62. https://doi.org/10.1016/j.geomorph.2016.07.025

References From the Supporting Information

Allen, J., Somerfield, P., & Gilbert, F. (2007). Quantifying uncertainty in high-resolution coupled hydrodynamic-ecosystem models. *Journal of Marine Systems*, *64*(1–4), 3–14.

Li, P., Yang, S. L., Milliman, J. D., Xu, K. H., Qin, W. H., Wu, C. S., et al. (2012). Spatial, temporal, and human-induced variations in suspended sediment concentration in the surface waters of the Yangtze estuary and adjacent coastal areas. *Estuaries and Coasts*, *35*(5), 1316–1327. https://doi.org/10.1007/s12237-012-9523-x

Pawlowicz, R., Beardsley, B., & Lentz, S. (2002). Classical tidal harmonic analysis including error estimates in MATLAB using T_TIDE. *Computers & Geosciences*, *28*(8), 929–937.

Richardson, J. F., & Zaki, W. N. (1954). *Sedimentation and fluidization: Part I, Trans* (Vol. 32, pp. 35–53). Institution of Chemical Engineers.